Review

Strategies to improve metal organic frameworks photocatalyst's performance for degradation of organic pollutants

Danni Jiang [a,b,1], Piao Xu [a,b,1], Han Wang [a,b,1], Guangming Zeng [a,b,*], Danlian Huang [a,b,*], Ming Chen [a,b], Cui Lai [a,b], Chen Zhang [a,b], Jia Wan [a,b], Wenjing Xue [a,b]

[a] College of Environmental Science and Engineering, Hunan University, Changsha 410082, PR China
[b] Key Laboratory of Environmental Biology and Pollution Control, Hunan University, Ministry of Education, Changsha 410082, PR China

ARTICLE INFO

ABSTRACT

Researches on metal-organic framework (MOF) materials have gathered increasing interest in the field of photocatalysis due to their large surface area, well-ordered porous structure, and tunable organic bridging linker/metal clusters with a tailorable capacity to absorb light. The development of inexpensive, stable, efficient, and band-gap tunable MOF-based photocatalysts is still a great challenge. The selection of central metal ions and organic ligands is of great importance for the fabrication of MOFs with excellent photocatalytic properties. This review aimed to summarize the strategies of improving photocatalytic activity under light illumination, including optimization, modification, doping and imperfection, mainly in structure, light absorption, band gap and stability. In addition, the applications of various modified MOFs are also introduced. Finally, the future developments of MOFs are discussed.

© 2018 Elsevier B.V. All rights reserved.

Contents

---

* Corresponding authors at: College of Environmental Science and Engineering, Hunan University, Changsha 410082, PR China.
E-mail addresses: zgming@hnu.edu.cn (G. Zeng), huangdanlian@hnu.edu.cn (D. Huang).
[1] These authors contributed equally to this article.

1. Introduction

Energy shortage is a serious social problem in the world today, which interferes with sustainable development [1,2]. Due to high utilization of light, heterogeneous photocatalysis has been seem to be a green and environmental, scientific and efficient method. Fujishima et al. devoted themselves to the pioneering work on the process of changing light energy to chemical energy by photocatalyst. Then, TiO_2 [3], ZnO [4], CdS [5] and Fe_2O_3 [6] as the representative of photocatalysts have been explored. Because of the limited tunable functionality and the instantaneous separation of electron-hole pair, the application of traditional semiconductor as photocatalyst is limited, and the researchers are devoting to develop novel, efficient, and tunable functional photocatalysts. Metal-organic frameworks (MOFs) in topological structure are built by the metal ions/clusters of inorganic secondary building units (SBU) and organic linkers with moderately strong coordination bondings [7,8]. Furthermore, as a result of precisely predesignable structures with tailored functionalities, MOFs are able to achieve structural and chemical control that are specific to target function. These merits along with structural diversities, abundant active sites, highly thermal stability and permanent porosities endow them great application potential in gas storage, separation, sensing and catalysis, as well as several other unrelated applications [9,10].

Recently, reviews have been made on various aspects of MOFs. Some reviews focus on structural strategies to fabricate the nanoparticle/MOF composites, including decoration of organic linker or metal center, combination with semiconductors and metal nanoparticles loading applied to different MOFs [11–13]. The mechanistic, functionality and structural complexity of MOFs are the emphasis in the review of Kuaila et al. [14]. The optical properties of MOFs can be flexible modulated via incorporation of NH_2 group, conductor photocatalysts like ZnO and metal sulfides nanoparticles, noble metal nanoparticles and graphene oxide (GO). Further, controllable design of tunable nanostructures (such as metal nanoparticles, quantum dots, polyoxometalates, organic and metallorganic molecules, biomacromolecules, and metal-organic polyhedra) inside MOFs for the versatile functions was summarized [15], with special emphasis on the preparation and synergistic properties of these composites. Notably, defect engineering in MOFs is an exciting concept for tailoring material properties, which opens up novel opportunities not only in sorption and catalysis, but also in controlling more challenging physical characteristics. The review done by Zhang et al. closed that gap by providing both a concise overview of defects in MOFs, or more broadly coordination network compounds (CNCs), including their classification and characterization, together with the potential applications of defective CNCs/MOFs. Others focus on environmental and energy applications [16]. Wang's [17] group summarized the photocatalytic degradation in metal organic frameworks, which emphasized on the reaction mechanism and the influence of various factors on the catalytic performance. Specially, Cr (VI) as a research object by the photocatalytic reduction of MOFs have got consummated [18]. Meanwhile, the study of photocatalytic mechanism, which is equal to highly convert energy into chemical energy, have draw the attention. The fundamental principles of energy transfer was summarized and the latest progress in energy transfer, light-harvesting, photocatalytic proton and CO_2 reduction, and water oxidation using MOFs was provided [19].

The review chosen common environmental pollutants: organic pollutants as a research object, aiming to summarize the strategies of improving photocatalytic activity under light illumination, including optimization, modification, doping and imperfection. It is important to optimize the metal centers and appropriate ligand for photocatalytic activity. In addition, metal semiconductor and metal-free semiconductor, specially, graphene and carbon nitride doping with MOFs has been pampered recently. Defective MOFs with magnetic metal Fe, Co, Ni are not only beneficial to the separation and recovery of materials, but also helpful to improve the photocatalytic ability. Secondly, the light absorption, band gap, stability and mechanism are emphasized. Finally, a personal perspective regarding the future developments of MOF is presented.

2. Optimization of MOFs photocatalyst

2.1. Optimization of MOFs photocatalyst on the basis of metal-clusters

MOFs emerged as a class of highly porous crystalline materials follow the principle of metal ions coordination with organic ligands [20,21]. As the core of the MOFs, the excited clusters are the main active sites of photocatalytic reaction, and it is important to choose the appropriate cluster to construct the MOFs with high photocatalytic activity [22]. Fe-based MOF materials taking (MIL-88A, MIL-53 MIL-68) as typical models on the basis of iron oxo-clusters may be a potential photocatalyst for dye degradation. MIL-53(Fe), a Fe (III) contained MOF build up from chains of Fe (III) octahedral and polycarboxylate ligands (1,4-benzenedicarboxylic acid), was endowed excellent optical properties. In the UV-vis, the band of MIL-53(Fe) at 224 nm is related with the ligand to metal charge transfer (LMCT) of O(II) = >Fe(III), which is derived from carboxylate oxygen to metal. Except the main peak, due to the transition in Fe(III), a small peak centered at 445 nm appears in MIL-53(Fe). By calculation, the band gap of MIL-53(Fe) is 2.72 eV which corresponds to absorption band edge [23]. The direct excitation of iron-oxo clusters is deemed as the main active site of photocatalytic reaction because of adsorption incident photons by the iron-oxo cluster instead of organic linker in MIL-53(Fe) [24]. Along with the generation of holes, the absorption of solar energy induces chemical reactions, showing that the photocatalytic cavitation is mainly responsible for the degradation of dyes. By changing the ration of precursor $FeCl_3 \cdot 6H_2O$ and ligand H_2BDC, MIL-53(Fe) changed to MIL-68(Fe) as a photocatalyst. The band in the low energy region between 452 and 600 nm is attributed to the $d \rightarrow d^*$ transition of Fe^{3+} ions [25]. Slightly different from the MIL-53(Fe), the band gap of MIL-68(Fe) is 2.8 eV which corresponds to the absorption edge as 440 nm. However, consistent with MIL-53 (Fe), the iron-oxo cluster, not organic ligand are uses as excited cites that is responsible for the photocatalytic performance of MIL-68 (Fe). In addition, MIL-88A similar to MIL-68 (Fe) is also effective for decoloration of methylene blue (MB) under visible light [26]. The band gap is as low as 2.05 eV which corresponds to the extended absorption edge of 650 nm. However, MIL-88A showed inconspicuous photocatalytic activity, specially, the MB degradation rate is less than 20% within 20 min. The formed ·OH possesses with oxidation capacity is responsible for oxidizing the surface adsorbed organic molecules [27]. Meanwhile, with the aid of H_2O_2 electron donor, the photogenerated holes can generate more ·OH radicals which are helpful for the photocatalytic conversion of dyes. Different from (ST-MOF235) by traditional hydrothermal methods, MOF 235 crystals, a type of iron-based MOF, were synthesized using a microwave-assisted method was presented (MA-MOF235), which exhibits excellent photocatalytic activity for the degradation of rhodamine B (RhB) [28]. The main optimal absorption band for MA-MOF 235 and ST-MOF 235 were 650 nm and 640 nm, which is different from MOF 235. The band gap energies of MA-MOF 235 and ST-MOF 235 were estimated to be 1.94 eV and 1.98 eV, suggesting that the potential of to act as a photocatalyst. In the presence of catalyst and H_2O_2 without light irradiation,

the degradation efficiency of RhB is unconspicuous for both MA-MOF235 and ST-MOF235. However, the chromaticity of Rhodamine B was significantly reduced when using visible light as light resource. Thus, MOF 235, H_2O_2 and visible light irradiation are necessary for the enhanced photocatalytic activity for RhB degradation.

Zn, as d-block metal element, could also be used to construct ZIF-8, a typical class of MOF. In the work of Wang et al. [29], ZIF-8 a versatile MOF based on imidazolate ligands, was selected as a photocatalyst to decompose MB. In the presence of UV light, there is an electron transfer from the highest occupied molecular orbital (HOMO) to the lowest unoccupied molecular orbital (LUMO) in the ZIF-8. The HOMO is mainly contributed by N 2p bonding orbitals, and the LUMO is mainly contributed by empty Zn orbitals. Therefore, one electron was captured from water molecules, which was oxygenated into the ·OH active species, being responsible for the decomposition of MB. Due to the good coordination ability of copper clusters, the MOFs with the core of copper clusters is regarded as a typical representative photocatalyst [30]. A three MOF {[$Cu_9(OH)_6(bte)_2(sip)_4(H_2O)_3$]·$6H_2O$}$_n$ (1) (bte = 1,2-bis(1,2,4-triazol-1-yl) ethane, sip = 5-sulfoisophthalate) based on the unprecedented enneanuclear copper(II) cluster with the property of magnetic separation exhibited good photocatalytic activity for the degradation of cationic dyes methy orange (MO) under UV light irradiation [31]. In virtue of UV-vis light, the transferred electron from the highest occupied molecular orbital (HOMO) to the lowest unoccupied molecular orbital (LUMO) interacting with H_2O into ·OH radicals to complete the transformation of energy. A five-coordinated copper-based coordination compound $Cu_2(2,2'-bipy)_2(pfbz)_4$ (1) (where 2,2'-bipy = 2,2'-bipyridine; Tpfbz = pentafluorobenzoate) with the five atoms that approximately located in an equatorial plane as an excellent photocatalyst for methyl orange (MO) was synthesized [32]. A small amount of H_2O_2 as electron donor which can increase the photocatalytic activity Cu-based MOF (Fig. 1a). The carbonization of MO may be explained by two factors. On the one hand, according to the

valence bond theory, five-coordinated Cu II may coordinate to oxygen atoms from H_2O_2 molecules (Fig. 1b) to form ephemeral transition state I, II and III with six or seven-coordinated structure [33]. Then the transition state helps to beak the Cu—O bonds to generate ·OH, which degraded organic dyes by Fenton-like path [34,35].

Notably, different metal catalytic centers may have different influences on the photocatalytic activity. Three new three-dimensional (3D) framework structures based on the transition metal Co, Ni, Zn, respectively, employing the same dicarboxylate ligand 4,4'-oxybis-(benzoic acid), 4,4'-bipyridine, were compared [36]. The band gap are 3.11 eV, 3.89 eV and 4.02 eV for 1, 2, 3 respectively, which followed the order 1 < 2 < 3, and the order of degradation is 1 > 2 > 3. In another words, the degradation of all dyes follows the reverse order. Accordingly, there would be two vacant electrons in the HOMO and LUMO in the absence of the UV light. RhB is within a reasonable range and has an appropriate orientation to form transitional active complexes, which discourage the excited M^{2+} center from decaying to its ground state quickly. Thus, one α-hydrogen atom of the methylene group bonded to the electron-withdrawing nitrogen atom of RhB, which will give up its electron and this results in the cleavage of the C—N bond and stepwise N-deethylation of RhB. The excited electron must remain except that react with O_2 into ·O_2^- to fill the HOMO and subsequently accomplish further degradation of RhB.

MIL-53(M) (M = Fe, Al, Cr) with different metal clusters as photocatalyst was compared with the cases with UV-vis light and visible light irradiation. Different from the main optical absorption band in 320 nm for MIL-53(Al), 395 nm for MIL-53(Cr) is close to 455 nm for MIL-53(Fe), respectively, which corresponds to the band gaps (Eg) of 3.87 eV, 3.20 eV, 2.72 eV (Eg = 1240/wavelength) [37]. It is generally believed that there is a correlation between the amount of the adsorbed photos and the photocatalytic activity of a photocatalyst [38]. As altering the metal ion from metallic element Al to transition metal Cr and Fe, it is a reasonable explanation of the graduated increased absorption photons corresponding to the decreased bandgap. Then the MIL-53(Fe) with the narrowest band
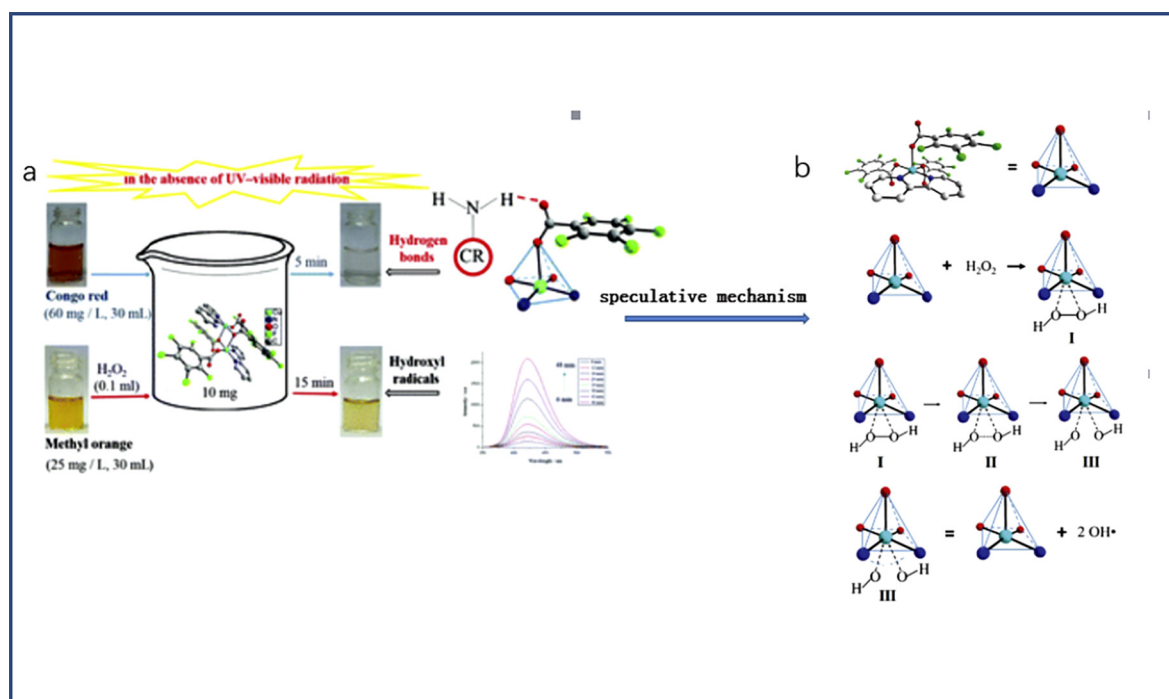

Fig. 1. (a) Synthesis route and catalytic performance of compound 1 and (b) the speculative mechanism of degrading MO (reprinted with permission from Ref. [32]. Copyright (2016) Royal society of chemistry).

Table 1

Recent studies on optimization and modification of the MOFs photocatalyst for improved photocatalytic activity.

On the basis of metal-clusters

MOF	Structure/Morphology	Absorption band edge	Band gap	Pollutant performance	Cycles	Mechanism	Reference
MIL-53Fe	Three dimensional framework	455 nm	2.72 eV	80% RhB was degraded	4	h+	[23]
MIL-68	Three dimensional framework	440 nm	2.80 eV		4	h+	[24]
MIL-88A	Hexagonal microrods	650 nm	2.05 eV	16% MB was degraded	4	·OH	[26]
MA-MOF235	Well-crystallized octahedral	650 nm	1.94 eV	RhB was completely decomposed within 20 min	3	h+, ·OH, ·O_2^-	[28]
ST-MOF235		640 nm	1.98 eV				
{[$Cu_9(OH)_6(bte)_2(sip)_4(H_2O)_3$]·$6H_2O$}$_n$	Two dimensional MOF	465 nm		76.1% MO was degraded	4	·OH radicals	[31]
Cu_2(2,2'-bipy)$_2$(pfbz)$_4$	Three dimensional MOF			85% MO was degraded		·OH radicals	[32]
[$Co_2(C_{10}H_8N_2)_2$][$C_{12}H_8O(COO)_2$]$_2$, [$Ni_2(C_{10}H_8N_2)_2$][$C_{12}H_8O(COO)_2$]$_2$, [$Zn_2(C_{10}H_8N_2)_2$][$C_{12}H_8O(COO)_2$]$_2$	Three dimensional MOF		3.11 eV / 3.89 eV / 4.02 eV	orange G, Rh B, Remazol Brilliant Blue R and MB was degraded		·OH radicals	[36]
MIL-53(M) (M = Fe, Al, Cr)	Well crystallized sphere-like particles	Fe 320 nm / Al 395 nm / Cr 455 nm	3.87 eV / 3.20 eV / 2.72 eV	Almost no difference on the same pollutant degradation		h+ and ·OH	[37]
{[Ni(SDB)(BITMB)(H_2O)]·H_2O}$_n$ (CP1), {[Cd(SDB)(BITMB) (H_2O)]·(THF)(H_2O)}$_n$ (CP2), {[Zn_2(SDB)$_2$(BITMB)]·(THF)$_2$}$_n$ (CP3) {[Co_2(SDB)$_2$(BITMB)](Dioxane)$_3$}$_n$ (CP4)	CP1 possesses one-dimensional ribbon type metal-organic motifs glued / CP2–CP4 exhibit non-interpenetrated sql networks	252 nm / 280 nm / 280 nm / 280 nm	2.12 eV / 3.89 eV / 4.08 eV / 2.11 eV	CP4 82.3% metanil yellow (MY)MY was degraded CP1 43.5%, CP2 24.7% CP3 51.9%			[39]
[$Mn_5(NH_2bdc)_5(bimb)_5$·(H_2O)$_{0.5}$]$_n$ (1), [Zn(NH_2bdc)(bix).(DMF)$_2$]n zene) (2), [Co(NH_2bdc)(bix)·(DMF)·(CH_3CH_2OH)]$_n$ (3) [Co(NH_2bdc)(bpp)]$_n$ (4)	MOF 1 displays 5-fold interpenetrating 4-connected dia 3D net; MOFs 2 and 3 are isomorphic, which possess 3-fold interpenetrating dia 3D nets; MOF 4 exhibits 4-connected sql 2D net	380 nm / 550 nm / 548 nm / 534 nm		Organic pollutants was degraded by MOF2		·OH radicals	[40]

On the basis of ligands

MOF	Structure	Absorption band edge	Band gap	Photocatalytic performance	Ligand	Mechanism	Reference
JUC-138	3D supramolecular structure	600 nm	3.34 eV	90% Decolorizing Azuce B was degraded within 4 h	Multi-carboxylic acid ligand		[42]
{[(CH_3)$_2NH_2$]$_3$(In_3L_4)}·(solvent)$_x$ (1)	Three periodic network	375–450 nm	2.89 eV	Decolorizing MB about 95.89% within 60 min Decolorizing MO about 92.80% within 120 min	carboxylate-based tritopic linker		[43]
[$Cu_2L_4(H_2O)_2$]$_n$	Three-dimensional supramolecular structures	490 nm		60% of RhB was degraded after 140 min	Multi-carboxylic acid ligand		[44]
Cu-II base MOF				A benzene conversion of 29%	Carboxyliate ligand	·OH	[45]
[Zn_5(Htea)$_2$(1,3-bdc)$_3$(H_2O)]·$2.6H_2O$	3D supramolecular structure			Photo oxidation of benzylamine to form N-benzylidenebenzylamine	Multitopic ligand	·O_2^-	[47]
{[$Zn_2(H_2O)$(1,4-ndc)$_2$(tpcb)]}$_n$ {[Zn(1,4-ndc)(tpcb)$_{0.5}$]}$_n$ {[$Zn_2(H_2O)$(2,3-ndc)$_2$(tpcb)]}$_n$		450 nm / 410 nm / 460 nm	2.62 eV / 2.90 eV / 3.34 eV	The photocatalytic efficiencies (3 > 2 > 1)	N-donor ligand	·OH	[48]
TMU-4 TMU-5 TMU-6	3D supramolecular structure	TMU-4 488 nm / TMU-5 585 nm / TMU-6 569 nm	TMU-4 2.6 eV / TMU-5 2.1 eV / TMU-6 2.2 eV	98.3% congo red was after 90 min	N-donor ligand	·OH	[49]

MOF	Structure	Absorption band edge	Band gap	Photocatalytic performance	Ligand	Mechanism	Reference
$[Co_2(L)(H_2O)_2(4,4'\text{-bipy})]\cdot 3CH_3CN$ (1) $[Mn_2(L)(1,10\text{-phen})(H_2O)]\cdot H_2O$ (2)	1 3D structure 2 2D layer structure			63.8% of methy violet (MV) was degraded within 100 min 72.5% of methy violet (MV) was degraded within 100 min	N-donor ligand	·OH	[51]
NNU-36	Pillared	650 nm	2.28 eV	96.2% of RhB was degraded after 70 min	bidentate N-donor ligand	·OH	[52]
$[Zn(2\text{-NCP})(3\text{-pyc})]_n$ $[Cu(2\text{-NCP})(3\text{-pyc})]_n$	3D supramolecular network structures		2.98 eV 2.76 eV	82% of MV, 80.41% of MO, 84.35% of MB and 70.86% of RhB have been decomposed after 190 min of irradiation for 2	N,O-donor ligands	·OH	[53]
$[Co2(1,4\text{-BDC})(NCP)2]_n\cdot 4nH_2O$ (1)	3D supramolecular network structure	200–800 nm		67.59% GO was degraded after 5 h	N,O-donor ligands		[54]
$[Co_5(mtpo)_2(\mu_3\text{-OH})_2(\mu_2\text{-OH})_2(COO)_3]$	3D framework			100% MB was degraded Within 140 min	N,O-donor ligands		[55]
MOF-1 MOF-2 MOF-3	MOF1.2 (4,4) type herrinbone grid MOF3 archetypal Kagomé topology		3.87 eV 2.301 eV 1.998 eV	88% of RhB was degraded for MOF-1, 91% for MOF-2 and 92% for MOF-3.	N,O-donor ligands		[56]
$\{[Cu(BIYB)_2(AQDA)]\cdot H_2O\}_n$	3D framework	336 nm 587 nm	2.65 eV	95% methylene blue was degraded after 50 min	Sulfonate ligand and azole ligand		[58]

On the basis of functional unit modified ligands

MOF	Absorption band edge	Band gap	Photocatalytic performance	Ligand	Mechanism	Reference
UiO-66-NH$_2$	477 nm	2.75 eV	Selective aerobic oxygenation of various organic compounds including alcohols, olefins and cyclic alkanes	Amine-functionalized ligand	·O$_2^-$	[61]
UiO-66-X (X = OH, NH$_2$, Br, (OH)$_2$, (SH)$_2$)	330 nm 350 nm 450 nm 480 nm 490 nm	UiO-66 3.91 eV UiO-66-Br 3.69 eV UiO-66-NH$_2$ 2.83 eV UiO-66-(SH)$_2$ 2.75 eV UiO-66-(OH)$_2$ 2.69 eV		Various functional ligand	·OH	[63]
MIL-125-NH$_2$ (X = —OH, —CH$_3$, —Cl)		MIL-125-CH$_3$/Cl 3.5 eV MIL-125-OH 2.8 eV MIL-125-NH$_2$ 2.6 eV		Various functional ligand		[68]

On the basis of polyoxometalates (POMs)

MOF	Absorption band edge	Band gap	Photocatalytic performance	Ligand	Mechanism	Reference
$(CH_3NH_2CH_3)[Cu_2(TPB)_2(PW_{12}O_{40})]\cdot 4DMF\cdot 6H_2O$			98.8% MO was degraded within two hours	POM-MOF host-guest hybrids	·O$_2^-$,·OH	[72]
$[Cu_3(4\text{-atrz})_8(PMo_{12}O_{40})2(H_2O)_2]\cdot 2H_2O$ (1) $[Cu_2(4\text{-atrz})_6(SiW_{12}O_{40})H_2O)]\cdot 6H_2O$ (2) $[Cu_2(4\text{-atrz})_4(\mu2\text{-OH})(CrMo_6(OH)_6O_{18})]\cdot 3H_2O$ (3) $[Cu_3(4\text{-atrz})_3(Mo_8O_{27})H_2O)_4]\cdot 6H_2O$ (4) $[Cu_3(4\text{-atrz})_3(V_{10}O_{30})0.5(\mu_3\text{-OH})(H_2O)]\cdot H_2O$ (5)			93.72% RhB was degraded for 1 28.76% RhB was degraded for 2 20.08% RhB was degraded for 3 16.57%RhB was degraded for 4 3.91% RhB was degraded for 5 after 180 min		·OH	[74]

gap among three MIL-53 photocatalysts is seemed as the most promising for MB degradation. Surprisingly, this exhibited almost no difference among three MIL-53 photocatalysts on the same pollutant. In the study of Bisht et al. [39], the significance of the metal clusters was confirmed based on angular dicarboxylate SDB and exobidentate N-donor ligand BITMB to assemble mixed ligand CPs with Ni^{2+}, Cd^{2+}, Zn^{2+} and Co^{2+}, corresponds to CP1, CP2, CP3 and CP4. CP1 comprises 1D metal organic ribbons, whereas, CP2-CP4 reveal sql type 2D sheets with pentagonal bipyramidal geometry at metal node for CP2, which are obviously different form paddlewheel secondary building units in the case of CP3 and CP4, this may be attributed to the coordination preferences of employed metal nodes and conformational flexibility of employed linkers in conjunction with weak noncovalent interactions. CP1 showed absorption band at 252 nm and CP2-CP4 showed the same at 280 nm. The band gap bridged from CP1 to CP4 of 2.12 eV, 3.89 eV, 4.08 eV and 2.11 eV, and the photocatalytic activity of metanil yellow followed the order CP2 < CP1 < CP3 < CP4. In addition, transition-metal centers ($Mn^{2+}/Zn^{2+}/Co^{2+}$) could coordinate with NH_2bdcH_2 and N-auxiliary ligands was prepared [40]. In the case of 3 and 4 based on the Co^{2+} ions, additional clear peaks in the visible region were observed at 548 (586) and 535 (583) nm, due to the d-d spin-allowed transition of the Co^{2+} ions, different from 3 and 4, the absorption of 1 exhibited in the visible region because of the d-d spin-forbidden of the Mn^{2+} ion. Compound 2 with absorption in the visible region (550 nm), different from other samples lie in the UV region, showed the highest photocatalytic activity. Therefore, the choice of metal center should be considered when designing the MOF as photocatalyst for catalyzing dye decomposition (Table 1).

2.2. Optimization of MOFs photocatalyst on the basis of ligands

Owing to strong coordination binds with metal ions, carboxylate, N-containing ligands or their co-ligand are often chose as building unit for the assemblage of stable and multifunctional coordination polymers [41]. A novel anionic metal-organic framework noted as JUC-138 on the coordination of a pyrene-based ligand, H_8TIAPy (H_8TIAPy = 1,3,6,8-tetrakis(3,5-isophthalic acid) pyrene) with In(III) was built for photocatalytic decolorization of Azure (AB). In JUC-138, the carboxyl groups are classified into two categories: four carbonyl groups connect to In^{3+} ions and uncoordinated ones. The stable 3D supramolecular structure of JUC-138 was build through the O—H...O hydrogen bonds between the uncoordinated carboxyl groups [42]. The energy gap Eg of JUC-138 is 3.34 eV according to UV-vis test, which contributed to high photocatalytic activity. In addition, a highly conjugated, carboxylate-based tritopic linker (H_3L = 5′-(5-carboxy-1H-benzo[d]imidazol-2-yl)-[1,1′:3′,1″-terphenyl]-4,4″-dicarboxylic acid) were chosen by Li et al. on the basis of a Indium-organic framework [43]. In-MOF has the characteristic of becoming a photocatalyst, and predominantly absorbs lights in the UV region of 200–375 nm as revealed by its diffuse reflectance spectrum, accompany by a faint visible absorption component ranging from 375 to 450 nm corresponding to band gap of 2.89 eV. The photocatalytic activity of In-MOF was reflected in MB and MO dyes until five experiments runs. In addition, flexible 3-(pyridine-2-yl)benzoic acid (HL) was chosen as multi carboxylic acid ligand where the carboxylate group of the ligand have multiple coordination sites. A new copper coordination polymer, $[Cu_2L_4(H_2O)_2]_n$ (1), (HL = 3-(pyridine-2-yl)benzoic acid) on the basis of HL has been solvothermally synthesized [44]. Compound 1 has a corresponding effect in the UV and visible regions. Originating from π-π^* transition of the L ligand, the weak absorption peaks at 250–360 nm in the UV region, besides, the intense absorption peaks at 490 nm in the visible region could be ascribed to the d-d spin-allowed transition of the

Cu (II) ions, thus, 1 shows good photocatalytic activity for carbonization of RhB. 5-(1H-Imidazol-1-yl)isophthalic acid (H_2L) was also a class of multi-carboxylic acid ligand. Based on the construction with H_2L and copper(II) ions, a Cu II based MOF was prepared [45]. The choice of solvents occupied an important position for catalysis hydroxylation of benzene to phenol. Waster was chosen as the sole solvent instead of the mixed solvents of the catalytic oxidation of benzene because a recent report indicated water could significantly accelerate the catalytic oxidation of benzene [46]. A benzene conversion of 29% as well as a high phenol selectivity above 95% has been obtained at 60 °C in water. The cycling tests showed no significant decrease after five runs, indicating good stability and reuse properties of the Cu II-based MOF. Under visible light irradiation, an excited charge separation occurred on the clusters in the Cu II based MOF (1) to offer an electron to Cu^{2+}, which was then reduced to Cu^+. The newly formed Cu^+ could reduce H_2O_2 to hydroxyl radicals in acidic conditions, then hydroxyl radicals are in charge of the catalytic reaction follows a Fenton-type route. Numerous multitopic ligands with multiple binding sites are after used to construct coordination polymers. A new coordination polymer has been obtained on the basis of a rigid ligand 1,3-benzedicarboxylic ligand acid in the presence of flexible ligand amino-alcohols:$\infty 3[Zn_5(Htea)_2(1,3-bdc)_3(H_2O)]\cdot 2.6H_2O$ (3) [47], the photocatalytic activity of which derived from the adsorption characteristics of the chromophore building blocks, leading to excited sites for photo oxidation of phenol and benzylamine with high substrate conversation rate and high product selectivity. Electrons are transformed from complex 3 to react with O_2 to generate $\cdot O_2^-$ and a positively charged compound (3^{*+}). Benzylamine reacts with the active with the $\cdot O_2^-$ to form benzaldehyde and ammonia, subsequently, the benzaldehyde can be converted to N-benzylidenebenzylamine. On the other hand, the use of flexible ligand could increase the water stability of MOFs, which is consistent with the study of Yang et al. [10]. Flexible MOF and rigid MOF should behave significantly different once the MOFs gradually take up water molecules: the flexible MOFs maybe able to adjust and self-adapt the frameworks themselves, leading to the formation of a new and successive hydrogen-bonding network for proton transportation during the transition states from fully activated MOFs to fully hydrated ones.

Because of the existence of the lone electron pair, the N-donor ligand is chosen as building unit for coordination polymers. In the case of N-donor ligands, tetrakis(4-pyridyl)cyclobutane (tpcb) is an excellent multidentate N-donor ligand in which four pyridyl groups could combine with metal ions with different conformations. Three novel Zn(II)/tpcb/dicarboxylate two dimensional (2D) and 3D coordination polymers based on the same tpcb for the photocatalytic degradation of MO and MB was compared [48]. The band gap increased from 1 (2.62 eV) to 2 (2.90 eV) to 3 (3.34 eV), and the photocatalytic efficiencies follow the reverse order (3 > 2 > 1). The faster generation speed of $\cdot$OH is related with the highest bandgap of 3, which leads to the faster decomposition of dye. Similarly, three zinc(II) metal-organic frameworks, $[Zn_2(oba)_2(4\text{-}bpdb)]$ (TMU-4), $[Zn(oba)(4\text{-}bpdh)_{0.5}]_n$ (TMU-5) and $[Zn(oba)(4\text{-}bpmb)_{0.5}]_n$ (TMU-6), (H_2oba = 4,4′-oxybisbenzoic acid, 4-bpdb = 1,4-bis(4-pyridyl)-2,3-diaza-1,3-butadiene,4-bpdh = 2,5-bis(4-pyridyl)-3,4-diaza-2,4-hexadiene and 4-bpmb = N^1,N^4-bis((pyridin-4-yl)methylene)benzene-1,4-diamine), containing azine-functionalized pores have successfully been synthesized on the basis of reaction of zinc metal salts with N-donor ligand [49]. The diffuse reflectance UV-vis spectroscopy fellows the order of TMU-4 (488 nm) < TMU-5 (585 nm) < TMU-6 (569 nm), corresponding to band gap of the MOFs as 2.6 eV, 2.1 eV, 2.2 eV respectively. Interestingly, TMU-6 shows the highest removal efficiency among other MOFs, which had no relation with the band gap. The use of different N-donor ligands with electron donating ability

to metal centers had led to different topologies and photocatalytic activities. Higher conjugated length of N-donor ligand in TMU-6 which causes the HOMO and LUMO to move closer, as well as higher surface area both contributed to maximum photo catalytic activity [50]. Lu et al. [51] presented both MOFs with different topologies due to the variation in the N-donor ligands have been applied as photocatalyst materials for the degradation of methy violet (MV). However, the catalytic activities of 1 and 2 are slightly different with the order of 2 (72.5%) > 1 (63.8%). These catalytic differences between 1 and 2 may be attributed to the difference in their $[M_2(CO_2)_4]$ geometry of the SBU and the high connectivity of the ligands. Complex 2 shows a better catalytic efficiency toward the MV degradation, which may be due to the better ability of Mn (II) ions to facilitate the formation of the hydroxyl radical (.OH) on the coordination network. Flexible bidentate N-donor ligands, such as bis (imidazole) 2 and bis (triazole) 3 ligands, are widely used to construct coordination polymers because flexible ligands can adopt different conformations according to the geometric needs of the different metal ions. As a kind of important organic ligands, the pyridyl benzota (pba) (including 4,4-pba, 4,3-pba, 3-3pba and 3,2-pba) have been used as multifunctional organic ligands, not only because of their various coordination modes, but also due to their ability to act as hydrogen bond acceptors and donors in the assembly of supra molecular structures [13]. A new visible-light driven MOF photocatalyst noted as NNU-36 has been rationally designed on the consideration of visible-light harvesting bipyridine ligand. The band gap of NNU-36 is estimated to be 2.28 eV through calculation of the band gap edge at 650 nm, which would has the potential to be a photocatalyst for dye degradation in a aqueous solution [52]. In the decolorizing process of the dye, the enhanced photocatalyst rate should be attributed to the efficient separation of electrons and holes, because the addition of H_2O_2 as electron acceptor used to eliminate electrons. In addition, the generated ·OH which is converted from H_2O_2 as oxidant to decompose dye molecules. The photo induced holes of NNU-36 played an oxidation role in the process of dye degradation. In addition, the photocatalytic activity of NNU-36 was demonstrated in four cyclic experiments.

Among the reported CPs, N,O-donor multifunctional ligands such as pyridine, carboxylic acids, pyrazine carboxylic acids, imidazole-4.5-dicarboxylic acids, and carboxyl derivatives of 1,10-phenanthroline are particularly interesting because of the change of multicoordination sites with metal ions. As an extension of the study of MOFs based on the carboxyl derivatives of 1,10-phenanthroline, Qiao [53] choose 2-(2-carboxyphenyl)imidazo(4, 5-f)-(1,10)phenanthroline (2-HNCP) and pyridine-3-carboxylic acid (3-Hpyc) mixed N,O-donor ligand to prepare the complexes of $[Zn(2\text{-}NCP)(3\text{-}pyc)]_n$ and $[Cu(2\text{-}NCP)(3\text{-}pyc)]_n$. The Eg values of 2.98 eV for 1 is slight higher than that of 2.76 eV for 2. Because mixed N,O-donor ligands can assume many kinds of bridging or chelating modes to construct thrilling CPs with novel structural motifs and interesting properties, and the complexes of $[Zn(2\text{-}NCP)(3\text{-}pyc)]_n$ and $[Cu(2\text{-}NCP)(3\text{-}pyc)]_n$ on the basis of N,O-donor ligands appear to be active for the photocatalytic decomposition of common organic dyes (MV, MO, MB and RhB) used in textile industries. A rigid benzene-1,4-dicarboxylic acid (1,4-H_2BDC) combine with 2-(4-carboxyphenyl)imidazo(4,5-f)(1,10)phenanthroline HNCP as mixed-linkers coordinate with Co^{2+} to generate a new coordination polymer $[Co_2(1,4\text{-}BDC)(NCP)_2]_n \cdot 4nH_2O$ (1) [54]. On one hand, HNCP with multiple sites is deemed as multifunctional ligand, which is extended to higher latitude topology. On the other hand, a large conjugated aromatic ring of HNCP can make it easy to extend into supramolecular structures through $\pi \cdots \pi$ conjugated bonds. Due to the optical properties of the large conjugated aromatic ring of HNCP, the absorption band of compound 1 extended from 200 nm to 800 nm, which facilitate excellent photocatalytic

degradation of multifarious artificial dyes as the representative of orange G (OG) under UV-vis irradiation. Also, the combination 7-Hydroxy-5-methyl-1,3,4-triazaindolizine (mtpo) with four potential coordination sites with terephthalic acid (H_2pdc) as building subunits is also a reasonable choice to prepare the cobalt (II) compound $[Co_5(mtpo)_2(pdc)_3(\mu_3\text{-}OH)_2(\mu_2\text{-}OH)_2(H_2O)_2]_n$ (1) for visible light driven photocatalytic degradation of MB [55].

Recently, low metal nucleatities are easy to construct the secondary building units (SBUs), however, it is difficult to control large cluster shape and nucleat suitable diffraction quality single crystals made SBUs with higher metal nuclearity. Pyrazole and various aromatic carboxylic acid ligands used as flexible ligand and rigid ligand respectively to design three Cu(II) MOFs (refer to MOF1, MOF2 and MOF3) with higher metal nuclearity was reported. All of them have good thermal stability and solvent stability and the band gap energies of which are 3.87 eV, 2.301 eV and 1.998 eV, respectively. Compare to MOF-1 and MOF-2, MOF-3 has both highest photocatalytic activity and magnetic properties which facilitates for easy isolation and circular use [56]. Compare with coordination polymers with carboxylate, N-containing ligands or their co-ligand systems [57], the attention degree of sulfonate-based assemblies is much small, despite the fact that the sulfonate group bears diversified coordinating modes and ligating sensitivity to the nature of the metal ions [58]. Wang et al. [59] try to combine the sulfoante ligands and azole ligands to explore novel Cu-based coordination polymer photocatalyst noted as $\{[Cu(BIYB)_2(AQDA)]\cdot H_2O\}_n$ (1), which photocatalytic convertion methyl blue which is resistant to light to small organic acids and CO_2.

3. Modification of MOFs photocatalyst

3.1. On the basis of functional units modified ligands

In sharp contrast to traditional semiconductors, the most obvious characteristic of MOFs exhibits excellent tunability properties [60]. Despite major breakthrough in the area of MOFs as photocatalyst, currently, it remains a big trial for researchers to development more efficient light-driven MOFs photocatalysts in a rational and systematic way, however, it is an effective strategy of incorporating functional metal centers or functional groups modified ligands into specific MOFs to address this challenge. A representative strategy to introduce catalytic sites is to make use of functional organic groups, such as —NH_2 —OH and —$(SH)_2$ decorated organic linkers.

An amine-functionalized as chromophore zirconium metal-organic framework (MOF) aims to expand the range of light absorption for a visible-light photocatalyst, which can be high efficiency and high selectivity for aerobic oxygenation of various compounds. The —NH_2 groups protrude into the micropores without sacrificing the topology. It is confirmed by comparing the uniform energies of Zr, C and O atoms in both UiO-66 and UiO-66-NH_2 [61]. The introduction of the chromophore amino group extended the absorption band to 477 nm corresponding to 2.75 eV and the positive slope of Mott-Schottky represented an n-type semiconductor. Using visible light sources, electrons on the HOMO composed of O, C and N 2p orbitals jump to the LUMO, and transfer to O_2 molecules to form .O_2^- radical, while the h^+ and the .O_2^- directly participated in photocatalytic degradation. Similarly, Shen [62] found a way to design multifunctional NH_2-mediated UiO-66, that is, by tuning the predesigned ligands with NH_2 functional groups, the optical absorption properties of coordination polymer MOFs can be flexibly modulated. The different functional ligand UiO-66-X (X = OH, NH_2, Br, $(OH)_2$, $(SH)_2$) applied different effects on the photocatalytic activity for Rhodamine B (RB) [63]. The bandgaps of UiO-66 (3.91 eV), UiO-66-Br (3.69 eV), UiO-66-NH_2 (2.83 eV), UiO-66-$(SH)_2$ (2.75 eV), and UiO-66-$(OH)_2$ (2.69 eV) were esti-

mated by the plot of $(\alpha h v)2$ versus energy (hv), which suggested that the bandgap of UiO-66 could be narrowed with different ligand functionalization. The BET surface areas of UiO-66-X (X = H, NH_2, Br, $(OH)_2$, $(SH)_2$) fellow the order of UiO-66-NH_2 (917 $m^2\,g^{-1}$) > UiO-66-H (835 $m^2\,g^{-1}$) > UiO-66-Br (563 $m^2\,g^{-1}$) > UiO-66-$(OH)_2$ (482 $m^2\,g^{-1}$) > UiO-66-$(SH)_2$ (418 $m^2\,g^{-1}$). In theory [64,65], the improved photocatalytic activity was related with larger surface ares with more active sites, in addition, which is ascribed to the narrow bandgap with stronger light absorption and excitation electronic activity. Interestingly, it is difficult to explain that abnormal phenomenon of UiO-66-$(SH)_2$ with the best photocatalyst activity compared with other catalysts by traditional theory [66]. So, UiO-66 $(SH)_2$ with excellent degradation performance derived from more active substances could decompose RhB effectively compared to UiO-66 (Fig. 2). With the help of chemical calculations, the work of Flage-Larsen et al. [67] explicitly illustrated that changes in the band gap were also observed by changing the coordination around the Zr atom, whereas isovalent substitutions on the metal center did not yield significant perturbations of the band gap. The first important conclusion of this study is that further lengthening past UiO-66 would indeed again reduce the band gap for the dehydroxylated cluster. The second important conclusion of this study is that there was significant difference on the band gap among UiO-66-H (4.0 eV), UiO-66-NO_2 (3.3 eV), UiO-66-NH_2 (2.9 eV), because of the electron density that would interact with the nitrogen lone pair states, yielding a reduced interaction between the two and less changes to the band gap. However, the oxygen atoms will have lone pairs, where only a slight reduction in the band gap can be seen. It is a future study to analyze the influence of of coordination environment of metal clusters on bandgap in combination with chemical calculation.

Hendon discussed band gap modification of MIL-125, a TiO_2/1,4-benzenedicarboxylate(bdc) MOF. When synthesized with the 1,4-benzenedicarboxylate (bdc) linker, MIL-125 has an optical band gap in the UV region (ca. 3.6 eV/345 nm) and is an active photocatalyst for the oxidation of alcohols to aldehydes [68]. This characteristic absorption pattern suggests that a single —NH_2 motif is responsible for the reduced band gap of the monoaminated series of MIL-125 analogues. The introduction of 10% bdc-R (R = —OH, —CH_3, —Cl) with different electron-donating capacity per unit cell resulted in flexible band gap control between 3.5 eV and 2.4 eV (Fig. 2). The weakest electron-donating group —CH_3, moderately decreases the band gap to 3.5 eV. The —OH group decreases the band gap to 2.8 eV, meanwhile, the —NH_2 group of the monoaminated bdc-NH_2 linker with strong electron-donating capacity could lower the bandgap of MIL-125 to 2.6 eV. Specially, the bdc-$(NH_2)_2$ linking unit was predicted to lower the bandgap of MIL-125 to 1.28 eV. It is easy to find that different functional ligands with different electron-donor capacities fellow the order of —$(NH)_2$ > —NH_2 > —OH > —Cl > —CH_3. The research shows that the modified ligand can narrow the band gap, however, it is not necessary related to the enhanced photocatalytic activity.

3.2. On the basis of polyoxometalates (POMs)

Polyoxometalate (POM)-based metal-organic framework (MOF) materials contain POM units and generally generate MOF materials with open networks. Because POMs are either directly part of the frameworks of MOFs or encapsulated within the cavities of MOFs, we called these kinds of materials POM-based MOF materials [69]. POM-based MOF single-crystal materials included: (i) d/f-block metal ion-modified POM units directly connected with organic ligands; (ii) POM anions residing within the cages of MOFs as templates; (iii) porous inorganic-organic materials with POM anions as pillars, and (iv) nano scale POM-based MOF crystalline materials. Lan and Su et al. employed a semirigid ligand containing eight carboxyl groups, 5,5'-(2,2-bis((3,5-dicarboxyphenoxy)methyl)propane-1,3-diyl)bis(oxy)diisophthalic acid (L1), to study the system of crystalline catalysts containing d10 metal-oxygen clusters. Fortunately, an unprecedented 3D heteropolyoxozincate organic compound with (3,4,24)-connected ddy topology, $[Zn_{16}(HPO_3)_4]L_{13}$ (IFMC-200), has been isolated, which is the first example of a 24-connected node constructed from a single d10 metal cluster. IFMC-200 exhibits superior thermal stability, good water stability, tolerance to acid and base [70]. Based on the nano cages or channels of MOFs, the unique coordination environments for POMs can be provided to form host-guest hybrid materials with fascinating photocatalytic properties. The POM-MOF host-guest hybrid materials could be obtained through two strategies. The guest of POMs directly assembled with metal cations and organic ligands in one-pot synthesis reactions, in addition, which can either be sojourned in the presynthesized MOFs with suitable nano pores. For the synthesis of POM-MOF hybrids, it is important to choose a suitable organic ligand because the geometry, length, and coordination ability of which all decide the frameworks structure. In the study of Zhao et al., two stable 3D polyoxometalate-based metal–organic framework (POMs), $[Cu^I_{12}(trz)_8(H_2O)_2][\alpha\text{-}SiW_{12}O_{40}]\cdot2H_2O$ (1) and $[Cu^I_{12}(trz)_8Cl][\alpha\text{-}PW_{12}O_{40}]$ (2) (Htrz = 1-H-1,2,4-triazole) based on Keggin-type POMs were successfully obtained. As nano active substance, polyoxometalate embedded in to nanopores of $[Cu^I_{12}(trz)_8(H_2O)_2][\alpha\text{-}SiW_{12}O_{40}]\cdot2H_2O$, on the other hand, polyoxometalate acted as building unit to construct $[Cu^I_{12}(trz)_8Cl]$ $[\alpha\text{-}PW_{12}O_{40}]$. The was significant differences in the photocatalytic activity toward RhB between 1 and 2, and the conversion of RhB increased from 20% to 91% for 1 and 81% for 1, respectively [71]. For example, a new host-guest POM-MOF hybrid material formu-
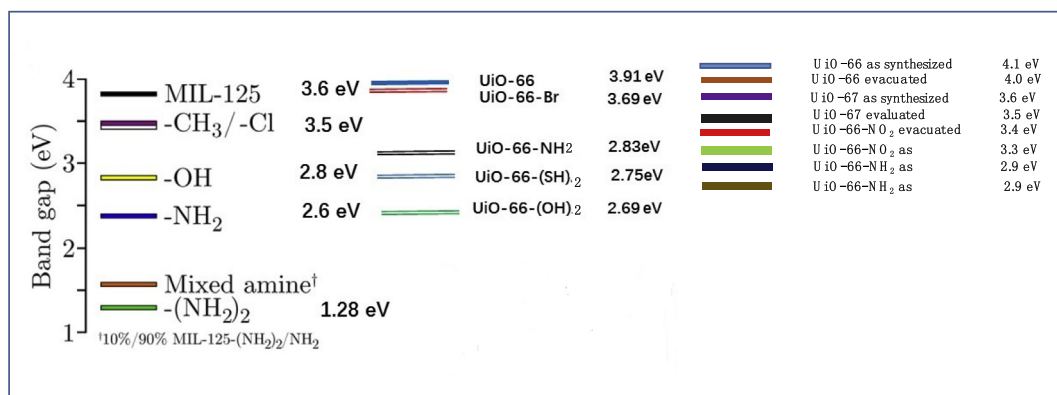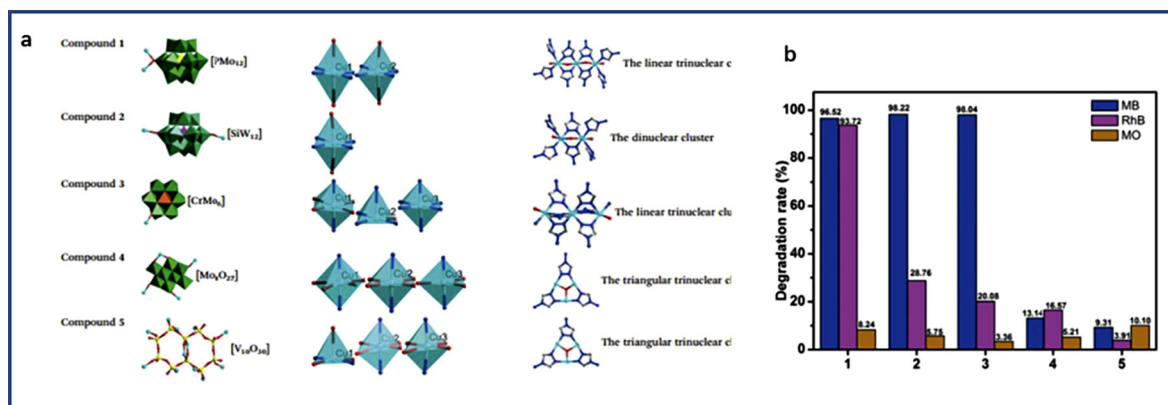

Fig. 2. The effect of different functional groups modified ligand on the bandgap of the MOFs.

Fig. 3. a. Coordination sites of POMs, coordination geometries of Cu(II) ions and the polynuclear Cu(II) clusters in 1–5; b. degradation rates of the MB, RhB and MO solutions in the presence of 1–5. (reprinted with permission from Ref. [74]. Copyright (2015) Royal society of chemistry).

lated as $(CH_3NH_2CH_3)[Cu_2(TPB)_2(PW_{12}O_{40})]\cdot4DMF\cdot6H_2O$ on the basis of 1,2,4,5-tetra(4-pyridyl)benzene (TPB) as a new rigid multifunctional ligand (1) that make it possible to realize host frameworks with specific topologies has been reported, which can realize 98.8% MO degradation within two hours [72]. The adsorbed H_2O_2 (major) and O_2 (minor) trap an electron in LUMO of the POM to generate oxidant radicals $\cdot OH$ and $\cdot O_2^-$, which are responsible for the oxidizing cationic dye methyl orange (MO). Similar photo-catalytic degradation of organic pollutant processes can be found in other POM-MOF systems [73].

In the finding of Wang et al., five POM-based MOFs containing various multinuclear clusters coordination with four types of POMs have been successfully compared [74]. By comparing the structures of 1–5, it is found that the lower dimensional compounds (1–3) on the basis of the linear multiclear Cu(II) clusters could be constructed in the presence of heteropolyanions, while higher dimensional compounds (4–5) was built on the principle of the triangular trinuclear Cu(II) clusters with the addition of isopolyanions (Fig. 3a). Compare to the high photocatalytic of lower dimensional compounds (1–3), while the higher dimensional compound (4–5) haven't shown obvious photocatalytic activity (Fig. 3b).
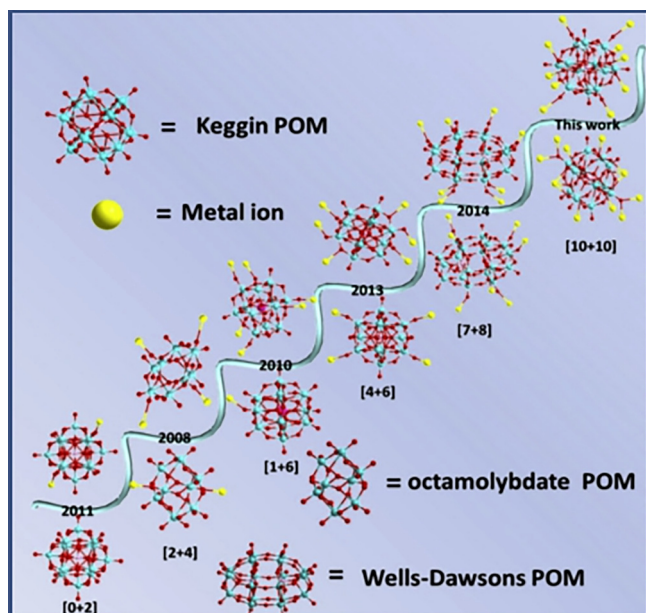
Recently, more and more researchers focus their attentions on POM@MOCs with complicated helical features because of their important applications in optical devices and asymmetric catalyst in material chemistry [75]. By the extensive studies about POM@MOCs with mixed-connected POM clusters, only octamolybdate, Keggin and Wells-Dawsons POMs as substrates are found, and the most complex mixed-connection of POMs is [7,8] connection to date. To assembly of the higher mixed-connected POM@MOCs, the 1,2,3-triazole (trz) ligands with smaller steric hindrance and more coordination sites are employed [76], and unprecedented POM@MOC with complex helical features, $[Ag_{28}(trz)_{18}][HPW_{12}O_{40}]_2$ ($Ag_{28}P_2W_{24}$), with [10,10] connected numbers was successfully fabricated. Interestingly, its polypyrrole (PPy) composites ($PPy/Ag_{28}P_2W_{24}$) has been prepared for good photocatalytic degradation for RhB dye under the visible light (Fig. 4).

4. Doping of MOF photocatalyst

4.1. On the basis of noble metal

Two key problems responsible for improved photocatalytic activity are the protection of the existence of photogenerated charge-carriers and improving the separation of photogenic electrons and holes. The highly reactive monodispersed metal NPs was controlled under the control of versatile binding sites of MOFs, which are expected to act as co-catalyst because of their high Fermi energy levels. Due to stable topology as well as photoresponse properties, MIL-100(Fe) is a competitive option to couple with Pd NPs by a facile alcohol reduction of precursor H_2PdCl_4 (Fig. 5(a)) [77]. As revealed in High-resolution TEM (HRTEM) image Fig. 5(b–d), the unchanged crystal structure of the MIL-100 (Fe) and the surface of which covered by the Pd NPs with the (1 1 1) plane (Fig. 5(e)) was observed. Moreover, compare to original MIL-100(Fe), the resulting Pd@MIL-100(Fe) due to synthetic effect has exhibited superior photoactivity toward the photocatalytic conversion of three typical PPCPs. The presence of Pd on the surface is convinient for interfacial charge transfer which would interfer with the combination of photogenic electrons and holes, thereby promoting a boost of photocatalytic activity. Further, the coexist of Pd and graphene oxide incorporated to MIL-101 as a selective photocatalyst used for the degradation of the triphenylmethane dye [78]. Except the Pd metal NPs as co-catalyst due to high Fermi energy levels, Au and Pt are the same. Efficient photocatalytic reduction of nitrobenzene was achieved by using a Pt-deposited amino-functionalised Ti(IV) metal-organic framework (Pt/Ti-MOF-NH_2) under visible-light irradiation [79] and the Pt

Fig. 4. View of the reported POM@MOCs based on mix-connected POMs.
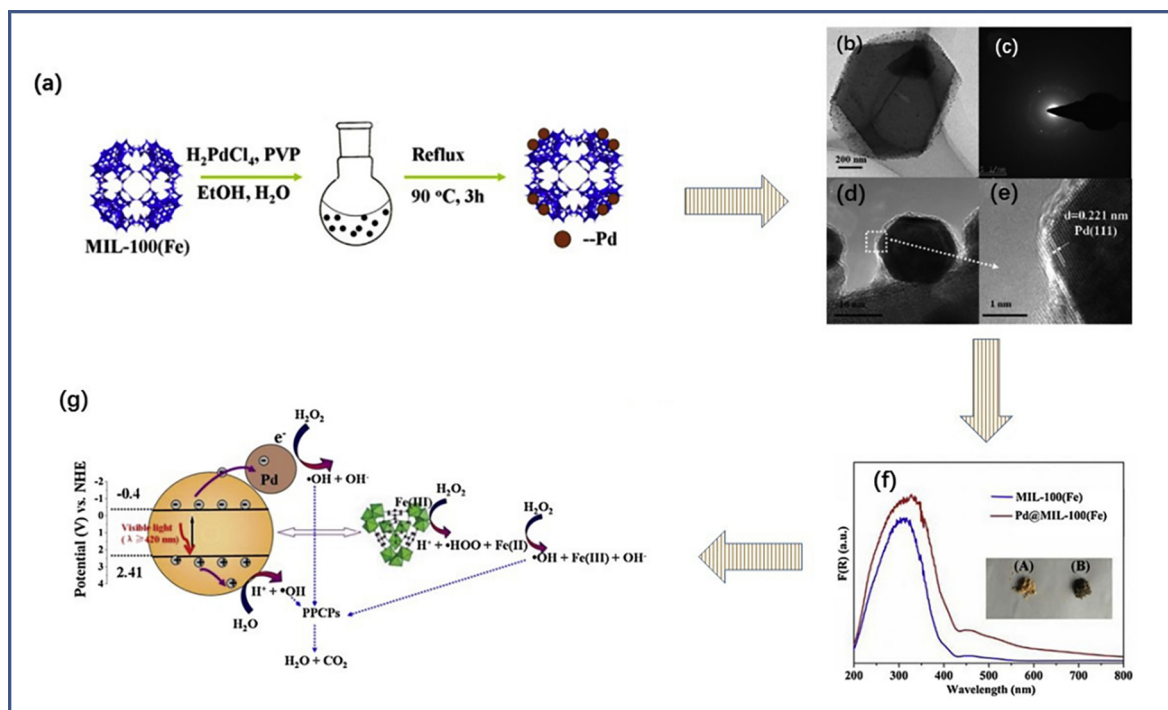
Fig. 5. (a) Overall flowchart for fabrication of the Pd@MIL-100(Fe) via a facile alcohol reduction approach; (b). TEM image (c). SAED pattern; (d and e). HRTEM image of the as-prepared Pd@MIL-100(Fe); (f). UV-vis DRS spectra of MIL-100(Fe) and Pd@MIL-100(Fe), the inset are the photographs of (A) MIL-100 (Fe) and (B) Pd@MIL-100(Fe); (g). proposed mechanism for the photocatalytic degradation of PPCPs over Pd@MIL-100(Fe) under visible light irradiation. (Reprinted with permission from Ref. [77]. Copyright (2015) Elsevier.)

act as a cocatalyst until five cycles. A set of noble-metal @MIL-100 (Fe) (M = Au, Pd, Pt) nanocomposites (denoted M@MIL-100(Fe)) was compared to improve the catalytic activity of MIL-100 (Fe) [80]. Under light source, the monodispersed noble-metal particles in M@MIL-100(Fe) as co-catalyst can capture the excited electrons and hinder the recombination with holes to improve the photocatalytic activity of MIL-100 (Fe). The integrity of the structure of MIL-100(Fe) after the photo deposition was observed from the SEM analysis (Fig. 6(a, b, d, e, g, h)), and XRD images (Fig. 6(c, f, i)) of the as-synthesised M@MIL-100(Fe) nanocomposites showed that

the post noble metal exists in the form of metal. In terms of photocatalytic performance, MIL-100(Fe) < Au@MIL-100(Fe) < Pd@MIL-100(Fe) < Pt@MIL-100(Fe), which fellow the reverse order of surface area. Accordingly, the enhanced visible light absorption, efficient charge-carrier separation as well we the synergistic effect all contribute to the higher photoactivity of M@MIL-100 (Fe). Both .OH derived from H_2O_2 and h^+ are major contributors to directly oxidize the adsorbed MO. Most importantly, the Fe(III)-O clusters on the surface of M@MIL-100(Fe) are responsible for the decomposition of H_2O_2 to produce more and more oxidative .OH radicals,
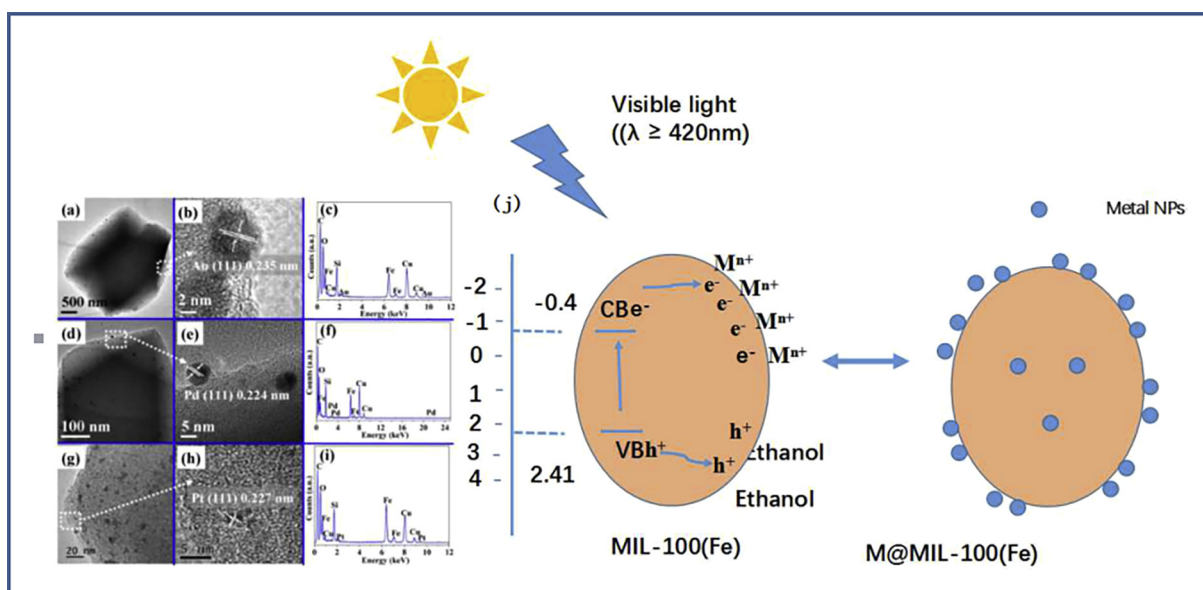
Fig. 6. TEM and HRTEM images of (a, b) Au@MIL-100(Fe); (d, e) Pd@MIL-100(Fe); (g, h) Pt@MIL-100(Fe), EDX images of (c) Au@MIL-100(Fe); (f) Pd@MIL-100(Fe); (i). Pt@MIL-100(Fe); (j) Photodeposition route for formation of M@MIL-100(Fe) nanocomposites. (Reprinted with permission from Ref. [80]. Copyright (2015) Springer.)

which is related with the oxidation and reduction of both dye and Cr(VI) under visible light irradiation ($\lambda \geq 420$ nm), as shown in Fig. 6(j).

4.2. On the basis of metal semiconductor

Considering the expensive cost and of the metal NPs and the complicate synthesis, the heterogeneous structure combination MOFs and semiconductor as photocatalysts presented significant advantages than the pure MOFs. As a result, semiconductor @MOF heterostructures beyond the function of monomers to produce new functions as a consequence of their synergistic effects.

The regulation of MOFs with semiconductor could affect the light absorption and the band gap of MOFs. ADA-Cd/TiO$_2$ was prepared by physically mixing original ADA-Cd crystals with TiO$_2$ at specific proportion, for the purpose of efficiently photo-degrade organic dyes under visible light irradiation. Interestingly, the band gap of ADA-Cd/TiO$_2$ is 3.14 eV, which is located between the 3.20 eV of TiO$_2$ and the 3.09 eV of ADA-Cd/TiO$_2$ [81]. The photocatalytic activities of TiO$_2$ or ADA-Cd towards organic dyes under visible light couldn't catch up with that of TiO$_2$ coordinated MOFs, indicating the synergistic between TiO$_2$ and ADA-Cd. In the cocatalyst system, electrons on the CB of TiO$_2$ oxidize O$_2$ from the ambient atmosphere to $\cdot$O$_2^-$ that acts as the main oxidative species in dyes photodegradation process, and h$^+$ left on the VB of ADA-Cd together with $\cdot$OH produced in alternative way play a secondary role. Zinc oxide (ZnO) is also an n-type semiconductor with many potential applications and heterostructured MOFs in combination with which have been reported. The core-shell heterostructure photocatalyst ZnO@MOF-46 with ZnO as the supplement of Zn^{2+}, which was for the formation of outer MOF-46 by dissolving inner ZnO in solvent mixtures, exhibited higher photocatalytic activity than pristine ZnO [82]. In fact, the formation of ZnO@MOF heterostructure was at the mercy of the balance between the dissolving rate of Zn^{2+} ions and their coordination rate with ligand. The band gaps of ZnO@MOF-46 as 2.44 eV is lower than ZnO as 3.23 eV, and MOF-46 as 2.72 eV. The $\cdot$O$_2^-$, $\cdot$OH and h$^+$ scavengers all involved and the $\cdot$OH take the biggest contribution to the pho-

tocatalyst process. It is the same as with the work of Rad and Dehghanpour, Wang [83] developed a similar strategy for rapid construction of core-shell ZnO@ZIF-8 heterostructure photocatalyst, and inner ZnO is used as the source of Zn^{2+} ions for formation of outer ZIF-8 Fig. 7(a). The concentration of organic ligand 2-methylimidazole (Hmim) was found to play an important role in the formation of ZnO@ZIF-8 core-shell heterostructures (Fig. 7(b–e)). In addition, reaction time is also a factor affecting the core-shell heterostructure. From the SEM image Fig. 7(f), 3 min is not enough for the whole reaction, because there are still some uncovered ZnO colloids spheres outside. It is right of 8 min to the fast fabrication of ZnO@ZIF-8 Fig. 7(g). However, the extended period to 20 and 60 min resulted in rough surface due to excessive organic ligand and there is no effect on the core-shell structure (Fig. 7(h, i)). The imbedment of ZnO in ZnO@ZIF-8 heterostructures could narrow the bandgap of ZnO@ZIF-8 to 3.24 eV, which is different from that of ZnO spheres (3.27 eV). The new photocatalyst could reduce or degrade both Cr(VI) and MB efficiently after 180 min irradiation, as shown in Fig. 7(j).

Cadmium sulfide (CdS) is the representative n type semiconductor [84,85] have been successfully decorated on the surface of MOF UiO-66(NH$_2$) via a facile photodeposition technique in a controlled manner. The photodeposition time of 6 h is very important for the formation of CdS, however, excessive photodeposition time make photocatalytic activity attenuate due to the large aggregates on the surface of the nanoparticles. The BET surface area representing the number of catalytic sites of CdS-U6 (322.61 m^2/g) is smaller than that of UiO-66 (NH$_2$) (756.04 m^2/g). Obviously, the specific surface area is not the key factor determining the photocatalytic activity. The excellent photocatalytic due to the charge injection from CdS into UiO-66 (NH$_2$) leads to efficient and longer charge separation by reducing the recombination of electron-hole pairs which was confirmed by free radical capture [86]. Similarly, in the work of Liang, [87], CdS-decorated MIL-68(Fe) nanocomposites also exhibited excellent photocatalytic response to converting 4-nitroaniline (4-NA) to p-phenylenediamine (PPD) in water. Due to the deposition of CdS, the S$_{BEC}$ changed from 206.58 m^2/g for MIL-68 to 142.82 m^2/g for CdS-M68 NCs. The photoexcited elec-
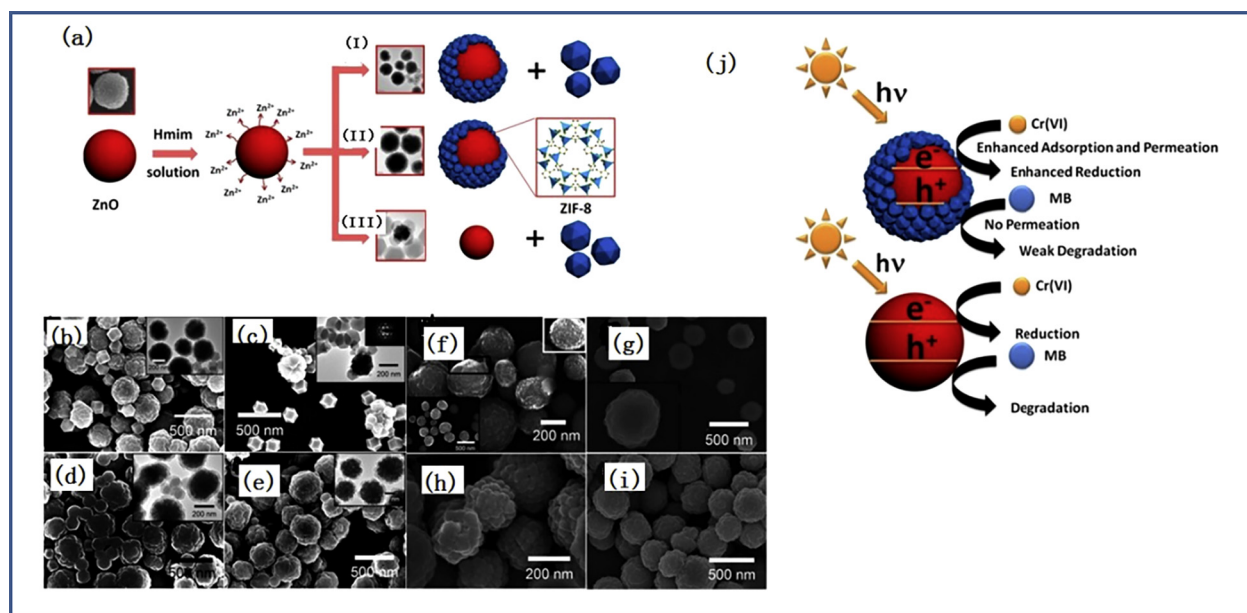
Fig. 7. (a) Schematic illustration of ZnO@ZIF-8 structure. SEM and TEM (inset) images of products obtained with different concentration of Hmim; (b) 4.51 M, (c) 1.83 M, (d) 0.915 M, and (e) 0.366 M; SEM images of the obtained products at different reaction times: (f) 3 min, (g) 8 min, (h) 20 min, and (i) 60 min; (j) schematic illustration of selectively enhanced photocatalysis properties of the ZnO@ZIF-8 core-shell heterostructures. (Reprinted with permission from Ref. [83]. Copyright (2016) American Chemical Society.)

trons and $\cdot CO_2^-$ radicals as the main active species inferred from the trapping experiments and ESR analysis are responsible for increased photocatalytic activity.

Bi-based semiconductor is considered as a potential photocatalyst [88,89], the composite materials with MOF could avoid the shortage of low utilization of photons, low adsorption capacity of Bi-based semiconductor [90,91]. The in situ growth of Bi-based MOF (CAU-17) on the support of thin sheet BiOBr 2D material was prepared. On the one hand, BiOBr acts as growth plate of MOF, on the other hand, which was also applied as Bi^{3+} sources of synthesized MOF [92]. In the presence of BiOBr/CAU-17, the dyes are sensitive to light and are degraded attributed to the good synergy effect.

Not only the BiOBr/CAU-17 heterostructured material but also BiOBr/NH$_2$-MIL-125(Ti) showed enhanced photocatalytic performance for dye degradation [93]. The absorption edges of the BiOBr/7 wt% NH$_2$-MIL-125(Ti) locate in the range of 425–435 nm, corresponding to band-gap energy (Eg) of approximately 2.70 eV. The surface area of BiOBr/7 wt% NH$_2$-MIL-125(Ti) is higher than that of BiOBr ($1.86 \ m^2/g$). The photo-generated electrons and injects electrons originated from conduction band of BiOBr transfer to the Ti^{4+} in the Ti—O (titanium oxo) cluster of NH$_2$-MIL-125(Ti) due to the heterojunction. In other words, $\cdot O_2^-$ and h^+ were the main active species for RhB photodegradation process. Similarly, BiOCl could take the place of BiOBr to incorporate with highly stable MOFs, UiO-66(Zr) by hydrothermal reactions. The resultant BiOCl/UiO-66 composite showed higher photodegradation performance of Rhodamine B (RhB) under ultraviolet and visible light irradiation than that of pristine materials and their mechanically mixed sample [94]. In addition, combination UiO-66(Zr) and Bi$_2$-MO$_6$ for the preparation of composites was also reported, and the support of Bi$_2$MO$_6$ has the effect of enlarging pore volume and BET surface area [95]. 2 wt% Bi$_2$MO$_6$ seems to the most suitable amount for the greatest photodegradation performance, but the excessive content of Bi$_2$MO$_6$ might lead to the decrease in the photocatalytic degradation efficiency. The photo-generated holes (h^+) as well as $\cdot O_2^-$ radicals as strong oxidant have participated in the redox process. By virtue of good stability, UiO-66 by optimizing to increase the sensitive of RhB to light was found in the study of Cheng et al. [96]. Similarly, CuWO$_4$ decorated into [CoNi(μ_3-tp)$_2$ (μ_2-pyz)$_2$] MOF as phtocatalyst to increase the sensitive of methylene blue (MB) to light [97].

The iron oxide nanoparticles encapsulated in the MOFs as photocatalyst, which are not only beneficial to improve the photocatalytic activity, but also facilitate for the magnetic separation [98]. Fe$_3$O$_4$ nanoparticles with the properties of both semiconductor and magnetic material encapsulated into flowerlike ZIF-67 was prepared, which used as excellent catalysis capacity for the fast magnetic removal of dyes from wastewater [99]. This broad absorption band ensured that the Fe$_3$O$_4$@ZIF-67 composites possessed strong photoabsorption ability in visible region that favored for the generation of photoinduced charges in the process of photocatalytic, which provided its potential as photocatalyst. The band-gap energy (Eg) of synthetic nanocomposite is 2.43 eV, which is different from the band gaps of 2.23 eV and 2.01 eV for pure Fe$_3$O$_4$ and ZIF-67. The good stability of the Fe$_3$O$_4$@ZIF-67 was verified in five cycles of Congo Red (CR) decolorization at the cost of the absence of Fe^{3+} ions. In addition, h^+ and $\cdot O_2^-$ are all related to the photocatalytic CR process. The aim of hierarchical nanostructures and heterojuctional construction through synthetic or computational screening has thus emerged with opportunities and challenges in the photocatalysis [100]. Similar to Fe$_3$O$_4$@ZIF-67, the core-shell structure is also applied to Fe$_3$O$_4$@MIL-100(Fe) for the photocatalytic oxidation of dyes [101].

A facile strategy was designed to obtain a novel type of hierarchical MOFs microspheres (NHMMs) that self-organized by ultra-thin MIL-88B(Fe) nanosheets, accompanying the embedment of Fe$_3$O$_4$ nanoparticles from the reduction of metallic nodes [102]. This strategy not only successfully achieves the simplified synthesis of iron-based MOFs in the form of hierarchical nanosheet structure, but also offers the magnetic integration into typical nanocomposite. Time plays a crucial role in the evolution of morphology and structure. Through 4 h hydrothermal reaction, the aggregated spheres no longer grow up as the ligand is exhausted. With the assistance of NaOAc, either the adsorbed free ferric ion or the metal nodes of MOFs in aggregated spheres can partially be converted to Fe$_3$O$_4$ nanoparticles, while this transformation process accompanying the consumption of intercalated Na-citrate also yields thinner and more flexible sheets (Fig. 8(a)). Meanwhile, through the attachment and coalescence of particles with citrate intercalated, oriented attachments proceed, yielding the larger spherical aggregates with surface wrinkles as illustrated in (Fig. 8(b)). With a prolonged reaction time to 10 h, the final hierarchical nanosheets stacked microspheres were obtained. The band gap energy is approximated to be 1.89 eV, thus, the dye (MB and RhB) photocatalytically degraded performance of the NHMMs/H$_2$O$_2$ system show distinct advantages under visible light, which is attributed to the combined effect of its special architecture, Fe$_3$O$_4$ generation that resulting in abundant micro/meso porous channels, wider absorption and efficient transport [103]. Under visible light irradiation, not only did implementing the semiconductor feature for the dye photodegradation together with H$_2$O$_2$ by MIL-88B(Fe), but also extending photoresponding range caused by the embedded Fe$_3$O$_4$ NPs. The iron-oxo clusters in MOFs could capture instantaneous photoelectron to produce the transition and transfer of electrons [104]. The hole subsequently is delocalized to the neighboring organic linkers which could trap the photogenerated holes at the aromatic linkers, achieving exceptional separation efficiency of photocarriers. Alternatively, the hierarchical nanosheet structures, which furnished abundant micro/meso porous channels, could contribute immensely to the transfer of electrons and holes generated inside the crystal to the surface and facilitate the dye degradation. Moreover, $\cdot$OH derived from the reaction of H$_2$O$_2$ and photoinduced electrons suppressed the electron-hole recombination and enhancing photocatalytic activity (as shown in Fig. 8(c)). Furthermore, this hybrid catalyst can maintain the stability and photocatalytic activity until the fourth photocatalytic cycle.

4.3. On the basis of metal-free semiconductor

Different from the above mentioned metal semiconductor, owing to the 2D network with high specific surface area beneficial for charge carrier mobility is also commonly chosen to adjust the bandgap of MOFs [105]. It is effective to avoid the problem by easy recombination of photogenerated charge and holes with the combination of MOF with graphene. Zhang et al. explained the role of GO in increased photocatalytic performance of graphene hybridized one dimensional MIL-53 (Fe) toward degrading RhB [106]. During the mild synthesis process, the reduction of graphene oxide (GO) and the MIL-53 (Fe) crystallization proceeded simultaneously, which is beneficial to the transfer of photogenerated charge through effective contact interface avoiding the recombination of excited carriers. It can be seen that attributing to the good optical properties of graphenes, the absorption edge of composites expended to the range 500–800 nm. Correspondingly, the color of MIL-53(Fe) gradually deepen after the doping of GO. The supplement of H$_2$O$_2$ could induce electron transfer to generate more amounts of $\cdot$OH radicals for the accelerated photocatalytic course [107]. Different from the traditional hydrothermal method, MIL-53(Fe)-reduced graphene oxide (M53-RGO) nanocomposites have been successfully designed by an electrostatic self-assembly
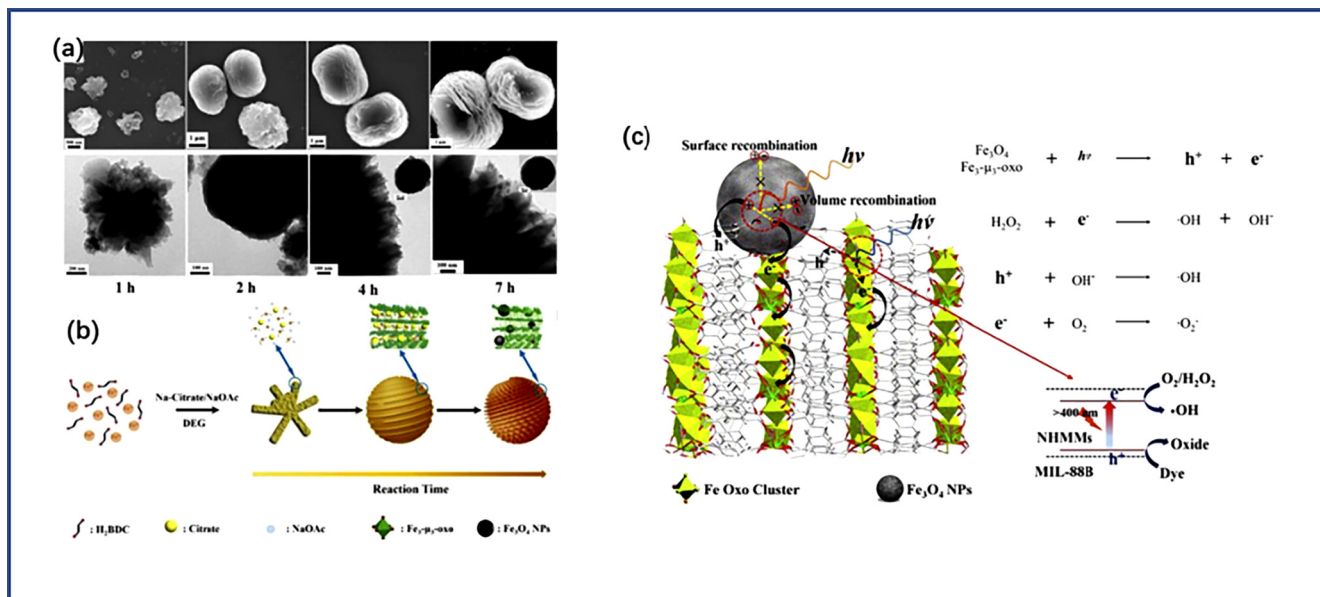
Fig. 8. (a) The morphology evolution of the HNMMs, typical SEM and TEM images at different reaction time; (b) the corresponding schematic illustration of the evolution process of the HNMMs; (c) schematic depicting the synergy of the NHMMs to harvest photos through energy transfer from the Fe_3O_4 NPs to the MOFs for the degradation of dye. (Reprinted with permission from Ref. [102]. Copyright (2016) Wiley.)

strategy, different from the traditional hydrothermal method, it is more conductive to the interfacial contact between GRO and the MIL-53(Fe). The calculated optical band gap of M53-0.5% RGO is 2.72 eV by optical analysis which is corresponds to 455 nm in the visible light. Obviously increased photocatalytic activity got a reasonable explanation. On the one hand, the good conductivity of the RGO could deliver electrons quickly [108]. On the other hand, the surface of both MIL(Fe) and RGO could be considered as reaction sites and offers more catalytic challenges [109]. In addition to graphene, the graphene-like g-C_3N_4 is metal-free semiconductor used to construct heterogeneous structure [110,111]. Notably, g-C_3N_4 serves as new research dimension for the construction of a novel photocatalytic system, enabling it to become a new family of next generation light-driven composite nanomaterials for applications in solar energy conversion [112].

A novel visible-light-response g-C_3N_4/MIL-53(Al) photocatalyst was synthesized which based on the advantages of MOFs with large surface area and g-C_3N_4 with photocatalytic activity [113]. The g-C_3N_4 (20 wt%) in g-C_3N_4 (20 wt%)/MIL-53(Al) contributed to the reduced band gap from 3.56 eV of MIL-53(Al) to 2.6 eV of g-C_3N_4 (20 wt%)/MIL-53(Al). The g-C_3N_4 played an important role in the ability to reduce charge resistance and increased photocatalytic activity. The main reactive species $.O_2^-$, h^+ and $.OH$ all involved in RhB degradation over g-C_3N_4(20%wt%)/MIL-53(Al). Similarly, hybrid nanocomposites on the principle of Fe-based MOF and metal-free graphitic g-C_3N_4 as an excellent photocatalyst were developed [114]. The band gaps tend to turn narrow after the introduction of g-C_3N_4 from 2.732 eV of MIL-53(Fe) to 2.51 eV of 3 wt%g-C_3N_4/MIL-53(Fe). The similar function of g-C_3N_4 in both g-C_3N_4/MIL-53(Al) and g-C_3N_4/MIL-53(Fe) was found, in summary, the introduction of a certain amount of metal free g-C_3N_4 would reduce resistence to charge migration attributed to the good electrical conductivity, consequently resulting in the boost of photocatalytic activity (Table 2).

5. Imperfection of MOF photocatlyst

Compared with both dense and nanoporous inorganic materials, MOFs are based on relatively weaker interactions (coordinative

bonds, π-π stacking, hydrogen bond, and so on) and present numbers of intramolecular degrees of freedom. Just as there is flexibility in any molecular assembly, there is no such thing as a crystalline solid without defects. The most commonly observed effect was an incomplete activation of framework porosity—resulting in guest molecules blocking the nanopores and negatively impacting surface area and adsorption capacity and photocatalytic capacity.

Some of the most interesting and multifunctional properties of MOFs are inherently related with the secondary building units (SBUs) coordination sphere. Magnetic elements Fe, Co, Ni are incorporated into the SBUs, which not only give the MOFs magnetic properties, but also increase the photocatalytic activity by producing unsaturated sites. There are two main strategies to realize substantial of metal clusters. On the one hand, in the direct synthesis, Fe substituted MOFs using a hydrothermal method was reported by Vu et al. In the case of Fe-Cr-MIL-101, only highly purity and high crystallinity of synthetic products exist except that undetected Fe_2O_3 and other phases [115]. It can be concluded that Fe is really incorporated into MIL-101 framework from the XPS result and the recyclability of Fe-Cr-MIL-101 was confirmed because the iron leaching is negligible. The activation of H_2O_2 by Fe-Cr-MIL-101 can produce more amounts of $\cdot OH$ radicals, thus which responsible for enhanced degradation efficiency of RR195. An imperfection strategy by Cu doped was successfully also applied to endow the microporous material ZIF-67 excellent photocatalytic properties. The Cu-doped phase in Cu/ZIF-67 played an important role in the increased the BET and Langmuir surface areas and lower bandgap of ZIF-67, based on these properties, the Cu/ZIF-67 exhibited enhanced photocatalytic activity [116]. The observation of an increase of photocatalytic activity might be due to the dyes easily be trapped to defects in the presence of free Cu^+ guests in the pores. Similarly, bimetallic Co/Zn-ZIF used as an efficient visible-light driven photocatalyst for degradation of Indigo Carmine (IC) [117]. Co/Zn-ZIF showed an intense characteristic absorption band from 450 to 650 nm, which is assigned for the typical [4A2(F)-4T1 (P)] d-d transition in tetrahedral cobalt. Especially, Co/Zn-ZIF had very good catalysis performance in strong alkaline medium due to the more hydroxyl radicals. Reactive oxygen species (ROS)

Table 2

Recent studies on doping of the MOFs photocatalyst for improved photocatalytic activity

Doping of the MOFs photocatalyst								
MOFs	Structure/Morphology	$S_{BET(m2/g)}$	Adsorption edge	Band gap	Photocatalytic performance	Mechanism	Recycle	Reference
Pd/MIL-101	Pd NPs anchored on MIL-101(Fe)	Pd/MIL-101 2102 MIL-101 2006	445 nm		Three typical PPCPs was degraded	·OH	4	[77]
Pd/MIL-101/rGO	MIL-101 had been embedded into the wrinkling rGO lamellar structure		240 nm		Brilliant green was completely degraded by Pd/MIL-101/rGO at 15 min		5	[78]
Pt/Ti-MOF-NH$_2$		Ti-MOF-NH$_2$: 1101 mg/L Pd/Ti-MOF-NH$_2$ almost uncahnge-			Reduction of nitrobenzene was achieved		4	[79]
(Au, Pd, and Pt) NPs on the MIL-100(Fe)	(Au, Pd, and Pt) NPs exist predominantly in metallic form	Pd@MIL-100(Fe), 1822 Au@MIL-100(Fe) 1989 Pt@MIL-100(Fe) 1724	200–400 nm		Pt@MIL-100(Fe) > Pd@MIL-100(Fe) > Au@MIL-100(Fe) > MIL-100(Fe)	·OH, h$^+$	4	[80]
ADA-Cd/TiO$_2$	Rod-like crystals		400–500 nm	3.14 eV	100%RhB was degraded	·OH, h$^+$, ·O$_2^-$	3	[81]
ZnO@MOF-46	Core-shell heterostructure		416 nm	ZnO/MOF-46 2.44 eV	81% methylene blue was degraded	·OH, h$^+$, ·O$_2^-$		[82]
ZnO@ZIF-8	Core-shell heterostructure		200–400 nm	ZnO/ZIF-8 3.27 eV	20 mg/L 40% of methylene blue was degraded		3	[83]
CdS@UiO-66(NH$_2$)		CdS@UiO-66(NH$_2$) 322.61 UiO-66(NH$_2$) 756.04	490 nm		Selective oxidation of benzyl alcohol to benzaldehyde	·OH, ·O$_2^-$		[86]
CdS@MIL-68		MIL-68 206.58 CdS@MIL-68 142.82			100% 4-NA was reduced	·CO$_2^-$	4	[87]
BiOBr/CAU-17	2D material		425–435 nm	BiOBr 2.84 eV BiOBr/CAU-17 2.86 eV	85.7% of RhB was degraded under visible light irradiation for 50 min	h$^+$, ·O$_2^-$	5	[92]
BiOBr/NH$_2$-MIL-125(Ti)	2D lamellar structure	BiOBr/NH$_2$-MIL-125 (Ti) 8.00 BiOBr 1.86	425–435 nm	BiOBr/NH$_2$-MIL-125 (Ti) 2.70 eV	80% of RhB was degraded for 100 min	h$^+$, ·O$_2^-$	4	[93]
BiOCl/UiO-66	The UiO-66 might attach on the BiOCL through chemical bonds	BiOCl 2.512 UiO-66 952.694 BiOCl/UiO-66 178.020	350 nm		20 mg/LRhB was degraded by the composite within 12 min	·O$_2^-$, h$^+$, ·OH	5	[94]
Bi$_2$MoO$_6$/UiO-66(Zr)	Heterojunctions	Bi$_2$MoO$_6$ 11 UiO-66 621 BMUO-0.5 726	505 nm	Bi$_2$MoO$_6$ 2.45 eV UiO-66(Zr) 3.65 eV	BMUO-2 shows the greatest photodegradation performance for RhB	h$^+$, ·O$_2^-$	3	[95]
UiO-66/ BiVO$_4$	Heterojunctions	BiVO$_4$ 14.7 UiO-66 646.4 UIO-66@BiVO$_4$-1 387	420–550 nm	UiO-66@BiVO$_4$ 2.8 eV	RhB was degraded under visible light irradiation	·O$_2^-$, h$^+$, ·OH		[96]
MOF/CuWO$_4$	Heterojunctions		470 and 550 nm	MOF/CuWO$_4$ 2.4 eV	98% of MB was degraded	·O$_2^-$, h$^+$, ·OH	6	[97]
Fe$_3$O$_4$/ZIF-67	Core-shell structure		708 nm	Fe$_3$O$_4$/ZIF-67 2.43 eV	72% of MB was degraded	h$^+$, ·O$_2^-$	3	[99]
Fe$_3$O$_4$/MIL-100	Core-shell structure	511.42 m^2 g	485 nm		99.77% of MB was degraded	h$^+$, ·OH	5	[101]
Fe$_3$O$_4$/MIL-88	Fe$_3$O$_4$ in micro/meso porous channel			Fe$_3$O$_4$/MIL-88 1.89 eV	99.8% of RhB was degraded after 80 min	·OH	4	[102]
GO/MIL-53	Two-dimensional nanosheet		455 nm	GO/MIL-53 2.72 eV	20 mg/L RhB was degraded within 60 min		3	[106]
g-C$_3$N$_4$/MIL-53	Two-dimensional nanosheet		348–450 nm	g-C$_3$N$_4$/MIL-53 2.51 eV	100% RhB was degraded after 75 min	·O$_2^-$, h$^+$, ·OH	5	[113]

including superoxide ($\cdot O_2^-$), singlet oxygen ($1O_2$), peroxide (H_2O_2) and hydroxyl radicals ($\cdot OH$) are responsible for the breaking the IC structure into simpler compounds.

On the other hand, post-synthetic partial substitution has been highlighted as an excellent strategies for improved photocatalytic activity and functionally diverse coordination polymers. Al^{3+} and Fe^{3+} substitution of MIL-101(Cr) came true using the PSM modification. Interestingly, when Al^{3+} is added to the MIL-101(Cr) the peak shifts from 592 nm to 602 nm because Al is a p-metal, however, Fe^{3+} substitutions is the opposite and the peak shifts to 585 nm because Fe have occupied d orbitals. This implied that Al^{3+} and Fe^{3+} with different electronic structure have opposite effects on the Cr(III)-BDC d-d transitions [118]. Post-synthetic modified samples slightly higher quadrupole splittings were measures than in the case of the pristine MIL-101(Fe), which is indicative of a less symmetrical arrangement around the ferric centers, not so surprising considering that the SBUs are no longer built up of the same trimetric Fe_3O clusters replaced by $FeCr_2O$. Fe(III) as transition metal ions for modification of MOFs has been widely reported because that plays an important role in increasing photocatalsis. The redox potentials of $Fe^{3+/2+}$ is lower than that of conduction band, in another word, the photogenerated electrons from photocatalysts can be easily trapped in the trap produced by the modified Fe(III) ions. On the other hand, Fe(III) ions were used as like-Fenton reagents to promote the photocatalytic oxidation. Shi et al. [119] successfully incorporated Fe(III) into the porphyrin unit (Fig. 9(j)) in PCN-224 with micrometer size cubic crystals ((Fig. 9(a, b)), importantly, iron is evenly embedded in porphyrin rings of PCN-224 ((Fig. 9(c–i)). Compared to the PCN-224, the photocatalytic oxidant activity for pollutant isopropanol (IPA) by the synthetic Fe@PCN-224 was increased by an 8.9 fold improvement. On one hand, the higher surface area make more active sites exposed. On the other hand, the implantation of Fe (III) ions in PCN-224 as trapping agent to separate the electron-hole, but also as a reactant in Fenton reaction produce reactive $\cdot OH$, which responsible for the oxidation of IPA ((Fig. 9(j)).
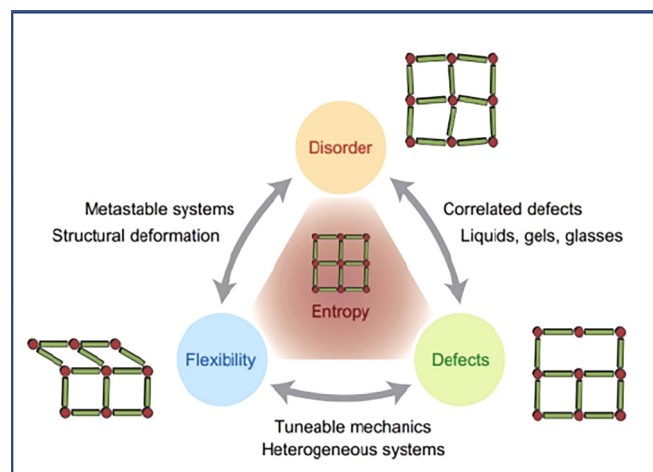

Fig. 10. Flexibility, defects and disorder in metal-organic frameworks. (Reprinted with permission from Ref. [124]. Copyright (2016) Elsevier.)

Efforts were made by Tu [120] toward facilitating the fast incorporation of transition element titanium into UiO-66 via cation exchange using micro-assisted method. From the analysis of optical properties, the calculated band gap of UiO-66 is 3.75 eV which is different from that of pristine UiO-66. Excitingly, the photocatalytic activity of UiO-66 was tremendously improved after the incorporation of Ti into UiO-66 because the photo electrons could be trapped more effectively by Ti act as electron traps, in addition, the incorporated Ti easier to absorb light electrons could then transfer them to neighboring Zr(IV). Therefore, due to the incorporation of transition metal Ti, it is convenient for the charge to transfer from photo-excited BDC to Zr—O oxoclusters, which would be favorable for a boost of phocatalytic performance.

In the defective Cd-MOF, the core metal Cd was intercalated with different valence metal ion, such as Ag^+, Zn^{2+} and Fe^{3+} as a representative by ion-exchange [121]. From an optical perspective,
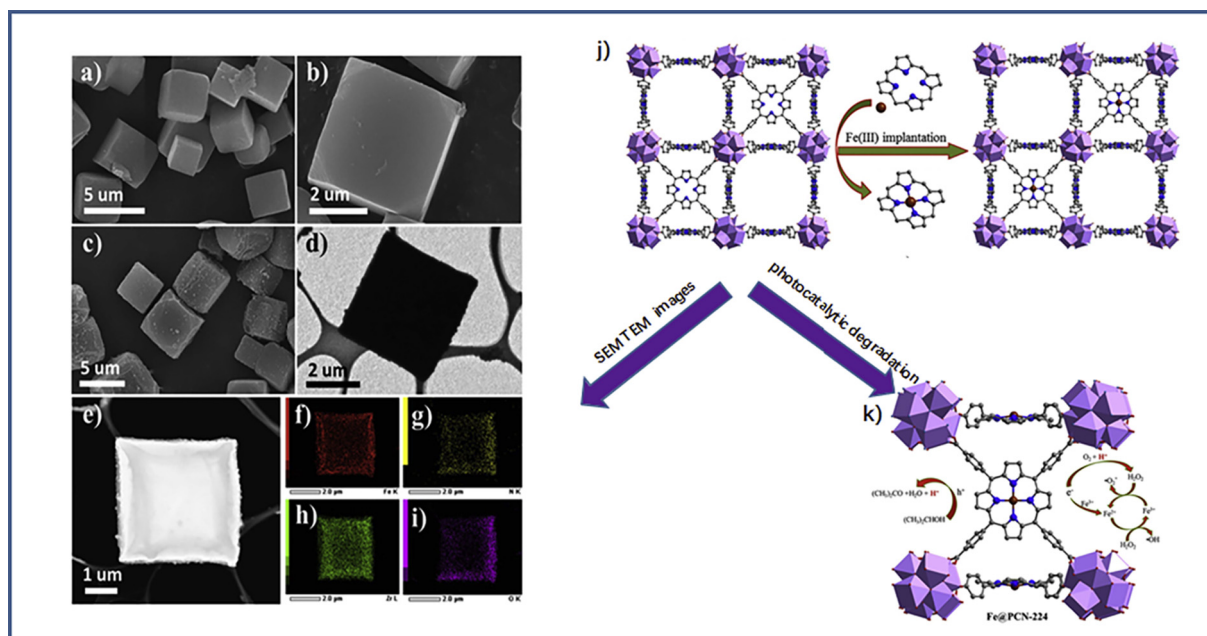

Fig. 9. (a)-(b) SEM images of PCN-224; (c)-(d) SEM and TEM images of Fe@PCN-224, respectively; (e)–(i) HAADF-STEM image and its corresponding elemental mapping images of Fe@PCN-224. (f) Fe, (g) N, (h) Zr, (i) O; (j) view of the 3D network of PCN-224 featuring highly porous framework as well as the implantation of Fe(III) sites into the PCN-224 framework; (k) proposed mechanism in photocatalytic systems with Fe@PCN-224. (Reprinted with permission from Ref. [119]. Copyright (2017) Elsevier.)

the band gap of Cd-MOF was estimated to be 3.6 eV, whereas those for the defective MOFs with Ag^+, Zn^{2+} and Fe^{3+} were 3.5 eV, 3.4 eV and 2.0 eV, respectively. Among these MOFs, Fe-Cd MOFs showed the optical photocatalytic degradation 93% of 2-CP which was attributed to the follow factors: on the one hand, the energy gap of Fe^{3+}-intercalated MOF is the lowest among these MOFs, on the other hand, introduction of Fe^{3+} significantly extended light absorption to the optical visible light zone.

Bimetallic Ni/Co based metal-organic framework with the magnetic $BiFeO_3$ have been successfully synthesized with the aid of facile synthesis approach, uniform and appropriate dispersion of magnetic $BiFeO_3$ on the rod-like MOF surface can be seen from the SEM images [122]. Eg values of the MOF, BiFeO3 and MOF/BiFeO3 were found to be 2.5, 2.1 and 2.3 eV, suggesting that the embedding of $BiFeO_3$ narrow the Eg values of the MOF. These results reveal that the prepared samples have the potential to act as a photocatalyst. It can be concluded that the h^+ and $\cdot OH$ radical were not the main involved species, however, $\cdot O_2^-$ mainly participated in the photo-degradation of MO dye ascribing to the EDTA-2Na scavenger. Notably, driven by optical and electrical properties, Mo(W)/Cu/S entity clusters as the core of MOF, has widely applied in photocatalytic degradation of dyes. A lot of productive efforts have been done by Yang's group on the synthesis and properties of visible-light-response heterobimetallic cluster $\{[WOS_3Cu_3Br(bip)_{2.5}]H_2O\}_n$ via the partial substitution [123]. With the help of H_2O_2, $\{[WOS_3Cu_3Br(bip)_{2.5}]H_2O\}_n$ showed effective photocatalytic performance on methylene blue (MB).

Flexibility, defects and disorder are all related to entropy (Fig. 9). They arise from the high dimensionality of the intramolecular degrees of freedom of the materials and the many corresponding 'soft' modes of low energy, as well as the relatively weak nature of the interactin involved in the framework assembly, such as coordinative bonds, π-π stacking and hydrogen bonds. Entropy also plays an important role in the formation of disordered MOF systems upon heating, and some MOFs proves to be a sufficient thermodynamic driving force to overcome unfavourable enthalpies of defect incorporation. Defects are disordered arrangements of atoms, and they caused the change in energy, which immediately represented in the change in the entropy. Combination of the chemical calculation to determine the change in the entropy and locate the defect active site is significant, which is also the focus of further research (Fig. 10 and Table 3).

6. Challenges and prospects

Due to cleanness and efficiency, solar energy has considerable potential for the degradation of organic pollutants. MOFs emerged as a novel class of controllable material with significant potential for photocatalysis. Commonly, photocatalytic activity can be increased by increasing the ability to convert photos, charge separation efficiency and more exposed catalytic sites. This review made a lot of efforts on the development involving the use of MOFs as photocatalysts, with particular summarization on several key strategies (i.e. optimization, modification, doping and imperfection), which is effective to improve the photocatalytic activity. Although remarkable achievements have been made on MOFs and MOFs composites as photocatalysts, and significant improvements are still required to improve the competitiveness of the MOF photocatalyst.

(1) The instability of MOFs which was attributed to the carboxylate ligands was easily replaced by water with higher affinities limited its application in aqueous solution. However, the hard metal ions (high valance metals) such as Fe^{3+}, Cr^{3+}, Al^{3+} and transition metal such as V^{4+}, Ti^{4+} and Zr^{4+} as the metal core coordination through strong binding force with hard bases containing donor atoms (O or N) tends to endow MOFs with satisfactory stability properties. In addition, the SUBs strategies was applied reasonably in the design and synthesis of MOFs, in other words, a dual-core or multi-core unit was designed with an excellent affinity between metal and nitrogen or oxygen, which is facilitate for more catalytic sites and multifunctional MOFs.

(2) Porphyrins and polyoxometalates are highly conjugated heterocyclic compound, which could response to visible light. In the design and synthesis of MOFs, porphyrins and

Table 3
Recent studies on imperfection of MOF photocatlyst for improved photocatalytic activity.

On the basis of metal clusters							
MOF	Structure/ Morphology	BET	Absorption band	Bang gap	Photocatalytic performance	Mechanism	Reference
Fe-Cr-MIL-101	Cubic shape	Cr-MIL-101 3532 Fe-Cr-MIL-101 2997			98% of RR195 was degraded after 100 min		[115]
Cu/ZIF-67				ZIF-671.98 eV Cu/ZIF-67 1.95 eV	100% of methy orange was degraded after 25 min		[116]
Co/Zn-ZIF	Powder of smaller crystal size		450–650 nm		100% of Indigo Carmine was decomposed after 3 h	$\cdot OH$, $\cdot O_2^-$ 1O2 H_2O_2	[117]
Fe-Cr-MIL-101 Al-Cr-MIL-101	Cubic shape		602 nm 585 nm			$\cdot OH$	[118]
Fe@PCN-224	Cubic shape	PCN-224 2726 Fe-pPCN-224 2360	1000 nm		Photooxidation of isopropanol (IPA)	$\cdot O_2^-$, $\cdot OH$	[119]
UiO-66	Pale brown crystals	UiO-66 969.7		UiO-66 4.00 eV	Photocatalytic reduction of Se(VI).		[120]
UiO-66(Zr/Ti)		UiO-66(Zr/Ti) 1264.3		UiO-66(Zr/Ti) 3.75 eV			
Ag$^+$-Cd-MOF	Prism-like structure	CdMOF 13.11		Cd-MOF 3.6 eV	93% of 2-CP was degraded by Fe^{3+}-Cd-MOF	$\cdot O_2^-$, $\cdot OH$	[121]
Fe^{3+} Cd-MOF Zn^{2+}-Cd-MOF				Ag$^+$-Cd-MOF 3.5 eV Fe^{3+} Cd-MOF 3.4 eV Zn^{2+}-Cd-MOF 2.0 eV			
Ni-CoMOF/BiFeO$_3$	Three dimensional rod-like morphology	Co-Ni-MOF 1058 Co-Ni-MOF/BiFeO$_3$			MO and 4-NP was photocatalytic degraded	$\cdot O_2^-$	[122]
$\{[WOS_3Cu_3Br(bip)_{2.5}]H_2O\}_n$	Bilayer 2D network				MB was degraded	$\cdot OH$	[123]

polyoxometalates were choose as building unite to enhance utilization of light source, which represents the further research direction.

(3) The leakage of metal ions and organic components from MOFs is a serious problem. Moreover, MOFs with low activity with the help of H_2O_2, peroxysulphate electron donor occupied large proportion. Thus, the high activity and high stability of MOFs are needed to avoid the above problems.

(4) Although the photocatalytic activity can be improved effectively with noble metal doping MOFs. Due to scarceness and valuableness, as well as easiness to be separated from MOFs, the noble metal in MOF as photocatalyst was under restrictions. In contrast, due to low cost, graphene and carbon nitride have excellent conductivity and special single atomic layer two-dimensional structure, which combination with MOFs could enhance the absorption of visible light, as well as the effective separation of photogenic electron and hole. Thus, doping metal-free semiconductor in MOFs becomes the new favorite of photocatalytic research. Specially, hetero atom doping in graphene or carbonized nitrogen with excellent photocatalytic activity combined with MOFs will be the focus of future researches.

(5) Magnetic metal such as Fe, Co and Ni substituted partial atoms to defective MOFs, which not only increased photocatalytic activity, but also gave the material magnetism that facilitate for separation and reuse. However, the photocatalytic performance and structure of defective MOFs have not been studied systematically, researches are needed to reveal the mechanism of defective MOFs.

(6) Most of the existing are concentrated in the degradation of organic pollutants, and the researches on other applications are needed.

Although many unsolved mysteries still exist in this area, the rapid development of MOFs as photocatalyst has become a new star in the field of material research. With the constant input of time and energy, it is envisaged that MOFs as photocatalyst will contribute to solving energy crisis.

Acknowledgements

References

[1] G. Zeng, M. Chen, Z. Zeng, Science 340 (2013) 1403.
[2] A. Kubacka, M. Fernándezgarcía, G. Colón, Chem. Rev. 112 (2012) 1555–1614.
[3] Y. Zhang, Q. Li, C. Liu, X. Shan, X. Chen, W. Dai, X. Fu, Appl. Catal. B (2017).
[4] C.Y. Su, A.M. Goforth, M.D. Smith, P.J. Pellechia, H.C. zur Loye, J. Am. Chem. Soc. 126 (2004) 3576–3586.
[5] S. Gao, W. Cen, Q. Li, J. Li, Y. Lu, H. Wang, Z. Wu, Appl. Catal. B 227 (2018) 190–197.
[6] L. Zhang, H.B. Wu, S. Madhavi, H.H. Hng, X.W. Lou, J. Am. Chem. Soc. 134 (2012) 17388–17391.
[7] J. Zhang, Y. Chen, X. Wang, Energy Environ. Sci. 8 (2015) 3092–3108.
[8] M. Marszewski, S. Cao, J. Yu, M. Jaroniec, Mater. Horiz. 2 (2015) 261–278.
[9] X.L. Lv, K. Wang, B. Wang, J. Su, X. Zou, Y. Xie, J.R. Li, H.C. Zhou, J. Am. Chem. Soc. 139 (2017) 211–217.
[10] F. Yang, G. Xu, Y. Dou, B. Wang, H. Zhang, H. Wu, W. Zhou, J.-R. Li, B. Chen, Nat. Energy 2 (2017) 877–883.
[11] J. Qiu, X. Zhang, Y. Feng, X. Zhang, H. Wang, J. Yao, Appl. Catal. B 231 (2018) 317–342.
[12] W. Xiang, Y. Zhang, H. Lin, C.J. Liu, Molecules 22 (2017).
[13] L. Shen, R. Liang, L. Wu, Chin. J. Catal. 36 (2015) 2071–2088.
[14] A. Kuila, N.A. Surib, N.S. Mishra, A. Nawaz, K.H. Leong, L.C. Sim, P. Saravanan, S. Ibrahim, ChemistrySelect 2 (2017) 6163–6177.
[15] L. Chen, R. Luque, Y. Li, Chem. Soc. Rev. 46 (2017) 4614–4630.
[16] L.-P. Ma, F. Zhao, L. Yao, X.-G. Li, D.-Q. Zhou, R.-L. Zhang, Angew. Chem. Int. Ed. 54 (2015) 7234–7254.
[17] C.-C. Wang, J.-R. Li, X.-L. Lv, Y.-Q. Zhang, G. Guo, Energy Environ. Sci. 7 (2014) 2831–2867.
[18] C.-C. Wang, X.-D. Du, J. Li, X.-X. Guo, P. Wang, J. Zhang, Appl. Catal. B 193 (2016) 198–216.
[19] T. Zhang, W. Lin, Chem. Soc. Rev. 43 (2014) 5982–5993.
[20] L. Qin, G. Zeng, C. Lai, D. Huang, P. Xu, C. Zhang, M. Cheng, X. Liu, S. Liu, B. Li, H. Yi, Coord. Chem. Rev. 359 (2018) 1–31.
[21] M. Cheng, C. Lai, Y. Liu, G. Zeng, D. Huang, C. Zhang, L. Qin, L. Hu, C. Zhou, W. Xiong, Coord. Chem. Rev. 368 (2018) 80–92.
[22] W. Xiong, G. Zeng, Z. Yang, Y. Zhou, C. Zhang, M. Cheng, Y. Liu, L. Hu, J. Wan, C. Zhou, Sci. Total Environ. 627 (2018) 235–244.
[23] R. Liang, F. Jing, L. Shen, N. Qin, L. Wu, J. Hazard. Mater. 287 (2015) 364–372.
[24] F. Jing, R. Liang, J. Xiong, R. Chen, S. Zhang, Y. Li, L. Wu, Appl. Catal. B 206 (2017) 9–15.
[25] G.T. Vuong, M.H. Pham, T.O. Do, Dalton Trans. 42 (2013) 550–557.
[26] W.T. Xu, L. Ma, F. Ke, F.M. Peng, G.S. Xu, Y.H. Shen, J.F. Zhu, L.G. Qiu, Y.P. Yuan, Dalton Trans. 43 (2014) 3792–3798.
[27] G. Liu, P. Niu, L. Yin, H.M. Cheng, J. Am. Chem. Soc. 134 (2012) 9070–9073.
[28] Y. Li, G. Hou, J. Yang, J. Xie, X. Yuan, H. Yang, M. Wang, RSC Adv. 6 (2016) 16395–16403.
[29] H.-P. Jing, C.-C. Wang, Y.-W. Zhang, P. Wang, R. Li, RSC Adv. 4 (2014) 54454–54462.
[30] O. Mehraj, F.A. Sofi, S.K. Moosvi, W. Naqash, K. Majid, J. Mater. Sci.: Mater. Electron. (2017) 1–12.
[31] X. Zhu, S. Zhao, Y.-F. Peng, B.-L. Li, B. Wu, CrystEngComm 15 (2013) 9154.
[32] L.J. Han, Y.J. Kong, T.J. Yan, L.T. Fan, Q. Zhang, H.J. Zhao, H.G. Zheng, Dalton Trans. 45 (2016) 18566–18571.
[33] J.Y. Xiang, J.W. Ponder, J. Comput. Chem. 34 (2013) 739–749.
[34] L. Liu, D. Wu, B. Zhao, X. Han, J. Wu, H. Hou, Y. Fan, Dalton Trans. 44 (2015) 1406–1411.
[35] D. Huang, C. Hu, G. Zeng, M. Cheng, P. Xu, X. Gong, R. Wang, W. Xue, Sci. Total Environ. 574 (2017) 1599–1610.
[36] P. Mahata, G. Madras, S. Natarajan, J. Phys. Chem. B 110 (2006) 13759.
[37] J.J. Du, Y.P. Yuan, J.X. Sun, F.M. Peng, X. Jiang, L.G. Qiu, A.J. Xie, Y.H. Shen, J.F. Zhu, J. Hazard. Mater. 190 (2011) 945–951.
[38] W. Dong, Y. Liu, G. Zeng, S. Zhang, T. Cai, J. Yuan, H. Chen, J. Gao, C. Liu, J. Colloid Interface Sci. 518 (2018) 156–164.
[39] K.K. Bisht, Y. Rachuri, B. Parmar, E. Suresh, J. Solid State Chem. 213 (2014) 43–51.
[40] L. Wen, L. Zhou, B. Zhang, X. Meng, H. Qu, D. Li, J. Mater. Chem. 22 (2012) 22603.
[41] S.L. James, Chem. Soc. Rev. 32 (2003) 276.
[42] N. Zhao, F. Sun, N. Zhang, G. Zhu, Cryst. Growth Des. 17 (2017) 2453–2457.
[43] Q. Li, D.-X. Xue, Y.-F. Zhang, Z.-H. Zhang, Z. Gao, J. Bai, J. Mater. Chem. A 5 (2017) 14182–14189.
[44] X.W.P. Wang, S.X.P. Lu, J. Inorg. Organomet. Polym Mater. 26 (2016) 1101–1106.
[45] L. Zhang, S. Qiu, G. Jiang, G. Jiang, R. Tang, Asian J. Org. Chem. 7 (2018).
[46] Y. Liu, T. Zhang, W. Wu, S. Jiang, H. Zhang, B. Li, RSC Adv. 5 (2015) 56020–56027.
[47] C. Paraschiv, A. Cucos, S. Shova, A.M. Madalan, C. Maxim, D. Visinescu, B. Cojocaru, V.I. Parvulescu, M. Andruh, Cryst. Growth Des. 15 (2015) 799–811.
[48] M. Dai, X.-R. Su, X. Wang, B. Wu, Z.-G. Ren, X. Zhou, J.-P. Lang, Cryst. Growth Des. 14 (2013) 240–248.
[49] M.Y. Masoomi, M. Bagheri, A. Morsali, RSC Adv. 6 (2016) 13272–13277.
[50] J. Gascon, M.D. Hernández-Alonso, A.R. Almeida, G.P.M. van Klink, F. Kapteijn, G. Mul, ChemSusChem 1 (2008) 981–983.
[51] L. Lu, J. Wang, S.L. Cai, B. Xie, B.H. Li, J.H. Man, Y.X. He, A. Singh, A. Kumar, J. Coord. Chem. (2017) 1–13.
[52] H. Zhao, Q. Xia, H. Xing, D. Chen, H. Wang, ACS Sustainable Chem. Eng. 5 (2017) 4449–4456.
[53] Y. Qiao, Y.-F. Zhou, W.-S. Guan, L.-H. Liu, B. Liu, G.-B. Che, C.-B. Liu, X. Lin, E.-W. Zhu, Inorg. Chim. Acta 466 (2017) 291–297.
[54] H.-Y. Sun, C.-B. Liu, Y. Cong, M.-H. Yu, H.-Y. Bai, G.-B. Che, Inorg. Chem. Commun. 35 (2013) 130–134.
[55] Y. Zhang, C. Zhao, H. Cui, Z. Anorg. Allg. Chem. 642 (2016) 1450–1453.
[56] S. Bala, S. Bhattacharya, A. Goswami, A. Adhikary, S. Konar, R. Mondal, Cryst. Growth Des. 14 (2014) 6391–6398.
[57] D.-S. Li, L. Tang, F. Fu, M. Du, J. Zhao, N. Wang, P. Zhang, Inorg. Chem. Commun. 13 (2010) 1126–1130.
[58] W.-J. Ji, Q.-G. Zhai, S.-N. Li, Y.-C. Jiang, M.-C. Hu, Inorg. Chem. Commun. 28 (2013) 16–19.

[59] X. Wang, Q.-G. Zhai, X.-Y. Hou, S.-N. Li, Y.-C. Jiang, M.-C. Hu, Inorg. Chem. Commun. 45 (2014) 1–4.

[60] Z. Wu, X. Yuan, G. Zeng, L. Jiang, H. Zhong, Y. Xie, H. Wang, X. Chen, H. Wang, Appl. Catal. B 225 (2018) 8–21.

[61] J. Long, S. Wang, Z. Ding, S. Wang, Y. Zhou, L. Huang, X. Wang, Chem. Commun. 48 (2012) 11656–11658.

[62] L. Shen, S. Liang, W. Wu, R. Liang, L. Wu, Dalton Trans. 42 (2013) 13649–13657.

[63] X. Mu, J. Jiang, F. Chao, Y. Lou, J. Chen, Dalton Trans. 47 (2018) 1895–1902.

[64] X. Zhou, C. Lai, D. Huang, G. Zeng, L. Chen, L. Qin, P. Xu, M. Cheng, C. Huang, C. Zhang, C. Zhou, J. Hazard. Mater. 346 (2018) 113–123.

[65] Y. Yang, C. Zhang, C. Lai, G. Zeng, D. Huang, M. Cheng, J. Wang, F. Chen, C. Zhou, W. Xiong, Adv. Colloid Interface Sci. (2018).

[66] C. Zhou, C. Lai, D. Huang, G. Zeng, C. Zhang, M. Cheng, L. Hu, J. Wan, W. Xiong, M. Wen, X. Wen, L. Qin, Appl. Catal. B 220 (2018) 202–210.

[67] E. Flage-Larsen, A. Røyset, J.H. Cavka, K. Thorshaug, Band gap modulations in UiO metal-organic frameworks, J. Phys. Chem. C 117 (40) (2013) 20610–20616.

[68] C.H. Hendon, D. Tiana, M. Fontecave, C. Sanchez, L. D'Arras, C. Sassoye, L. Rozes, C. Mellot-Draznieks, A. Walsh, J. Am. Chem. Soc. 135 (2013) 10942–10945.

[69] D.Y. Du, J.S. Qin, S.L. Li, Z.M. Su, Y.Q. Lan, Chem. Soc. Rev. 43 (2014) 4615–4632.

[70] D.Y. Du, J.S. Qin, Z. Sun, L.K. Yan, M. O'Keeffe, Z.M. Su, S.L. Li, X.H. Wang, X.L. Wang, Y.Q. Lan, Sci. Rep. 3 (2013) 2616.

[71] X. Zhao, S. Zhang, J. Yan, L. Li, G. Wu, W. Shi, G. Yang, N. Guan, P. Cheng, Inorg. Chem. 57 (2018) 5030–5037.

[72] M. Huo, W. Yang, H. Zhang, L. Zhang, J. Liao, L. Lin, C. Lu, RSC Adv. 6 (2016) 111549–111555.

[73] A. Tian, J. Liu, T. Li, Y. Tian, G. Liu, J. Ying, CrystEngComm 20 (2018) 2940–2951.

[74] X.-L. Wang, C.-H. Gong, J.-W. Zhang, G.-C. Liu, X.-M. Kan, N. Xu, CrystEngComm 17 (2015) 4179–4189.

[75] W.-W. He, S.-L. Li, H.-Y. Zang, G.-S. Yang, S.-R. Zhang, Z.-M. Su, Y.-Q. Lan, Coord. Chem. Rev. 279 (2014) 141–160.

[76] X.-Y. Yang, H.-F. Zhang, S.-X. Li, J.-Q. Sha, X. Li, F. Ma, Polyhedron 144 (2018) 240–248.

[77] R. Liang, S. Luo, F. Jing, L. Shen, N. Qin, L. Wu, Appl. Catal. B 176–177 (2015) 240–248.

[78] Y. W. Huo, L. Zhang, Environ. Sci. Pollut. Res. Int. 22 (2015) 17238–17243.

[79] T. Toyao, M. Saito, Y. Horiuchi, K. Mochizuki, M. Iwata, H. Higashimura, M. Matsuoka, Catal. Sci. Technol. 3 (2013) 2092.

[80] R. Liang, F. Jing, L. Shen, N. Qin, L. Wu, Nano Res. 8 (2015) 3237–3249.

[81] M.H. Xie, R. Shao, X.G. Xi, G.H. Hou, R.F. Guan, P.Y. Dong, Q.F. Zhang, X.L. Yang, Chemistry 23 (2017) 3931–3937.

[82] M. Rad, S. Dehghanpour, RSC Adv. 6 (2016) 61784–61793.

[83] X. Wang, J. Liu, S. Leong, X. Lin, J. Wei, B. Kong, Y. Xu, Z.X. Low, J. Yao, H. Wang, ACS Appl. Mater. Interfaces 8 (2016) 9080–9087.

[84] S. Gu, Y. Chen, X. Yuan, H. Wang, X. Chen, Y. Liu, Q. Jiang, Z. Wu, G. Zeng, RSC Adv. 5 (2015) 79556–79564.

[85] G. Chen, B. Yi, G. Zeng, Q. Niu, M. Yan, A. Chen, J. Du, J. Huang, Q. Zhang, Colloids Surf., B: Biointerfaces 117 (2014) 199–205.

[86] L. Shen, S. Liang, W. Wu, R. Liang, L. Wu, J. Mater. Chem. A 1 (2013) 11473.

[87] R. Liang, F. Jing, G. Yan, L. Wu, Appl. Catal. B 218 (2017) 452–459.

[88] C. Zhou, C. Lai, P. Xu, G. Zeng, D. Huang, C. Zhang, M. Cheng, L. Hu, J. Wan, Y. Liu, W. Xiong, Y. Deng, M. Wen, ACS Sustainable Chem. Eng. 6 (2018) 4174–4184.

[89] H. Wang, X. Yuan, Y. Wu, G. Zeng, W. Tu, C. Sheng, Y. Deng, F. Chen, J.W. Chew, Appl. Catal. B 209 (2017) 543–553.

[90] J. Wang, L. Tang, G. Zeng, Y. Deng, H. Dong, Y. Liu, L. Wang, B. Peng, C. Zhang, F. Chen, Appl. Catal. B 222 (2018) 115–123.

[91] Y. Deng, L. Tang, G. Zeng, J. Wang, Y. Zhou, J. Wang, J. Tang, L. Wang, C. Feng, J. Colloid Interface Sci. 509 (2018) 219–234.

[92] S.-R. Zhu, M.-K. Wu, W.-N. Zhao, P.-F. Liu, F.-Y. Yi, G.-C. Li, K. Tao, L. Han, Cryst. Growth Des. 17 (2017) 2309–2313.

[93] S.R. Zhu, P.F. Liu, M.K. Wu, W.N. Zhao, G.C. Li, K. Tao, F.Y. Yi, L. Han, Dalton Trans. 45 (2016) 17521.

[94] X. Tong, Z. Yang, J. Feng, Y. Li, H. Zhang, Appl. Organomet. Chem. 32 (2018) e4049.

[95] J. Ding, Z. Yang, C. He, X. Tong, Y. Li, X. Niu, H. Zhang, J. Colloid Interface Sci. 497 (2017) 126–133.

[96] C. Cheng, J. Fang, S. Lu, C. Cen, Y. Chen, L. Ren, W. Feng, Z. Fang, J. Chem. Technol. Biotechnol. 91 (2016) 2785–2792.

[97] H. Ramezanalizadeh, F. Manteghi, J. Cleaner Prod. 172 (2018) 2655–2666.

[98] P. Xu, G.M. Zeng, D.L. Huang, C.L. Feng, S. Hu, M.H. Zhao, C. Lai, Z. Wei, C. Huang, G.X. Xie, Z.F. Liu, Sci. Total Environ. 424 (2012) 1–10.

[99] W. Guan, X. Gao, G. Ji, Y. Xing, C. Du, Z. Liu, J. Solid State Chem. 255 (2017) 150–156.

[100] X. Feng, X. Chen, F. Jiang, J. Colloid Interface Sci. 494 (2017) 32–37.

[101] C.-F. Zhang, L.-G. Qiu, F. Ke, Y.-J. Zhu, Y.-P. Yuan, G.-S. Xu, X. Jiang, J. Mater. Chem. A 1 (2013) 14329.

[102] Z. Jin, W. Dong, M. Yang, J. Wang, H. Gao, G. Wang, ChemCatChem 8 (2016) 3510–3517.

[103] K.G. Laurier, E. Fron, P. Atienzar, K. Kennes, H. Garcia, M. Van der Auweraer, D. E. De Vos, J. Hofkens, M.B. Roeffaers, Phys. Chem. Chem. Phys.: PCCP 16 (2014) 5044–5047.

[104] K.G. Laurier, F. Vermoortele, R. Ameloot, D.E. De Vos, J. Hofkens, M.B. Roeffaers, J. Am. Chem. Soc. 135 (2013) 14488–14491.

[105] P. Samaddar, Y.-S. Son, D.C.W. Tsang, K.-H. Kim, S. Kumar, Coord. Chem. Rev. 368 (2018) 93–114.

[106] C. Zhang, L. Ai, J. Jiang, Ind. Eng. Chem. Res. 54 (2014) 153–163.

[107] D. Wang, F. Jia, H. Wang, F. Chen, Y. Fang, W. Dong, G. Zeng, X. Li, Q. Yang, X. Yuan, J. Colloid Interface Sci. 519 (2018) 273–284.

[108] X. Yuan, H. Wang, Y. Wu, G. Zeng, X. Chen, L. Leng, Z. Wu, H. Li, Appl. Organomet. Chem. 6 (2016) n/a–n/a.

[109] Z. Wu, X. Yuan, Z. Hua, W. Hou, G. Zeng, X. Chen, W. Hui, Z. Lei, J. Shao, Sci. Rep. 6 (2016) 25638.

[110] L. Jiang, X. Yuan, Y. Pan, J. Liang, G. Zeng, Z. Wu, H. Wang, Appl. Catal. B 217 (2017) 388–406.

[111] H. Wang, X. Yuan, Y. Wu, G. Zeng, X. Chen, L. Leng, H. Li, Appl. Catal. B 174–175 (2015) 445–454.

[112] W.J. Ong, L.L. Tan, Y.H. Ng, S.T. Yong, S.P. Chai, Chem. Rev. 116 (2016) 7159–7329.

[113] D. Guo, R. Wen, M. Liu, H. Guo, J. Chen, W. Weng, Appl. Organomet. Chem. 29 (2015) 690–697.

[114] W. Huang, N. Liu, X. Zhang, M. Wu, L. Tang, Appl. Surf. Sci. 425 (2017) 107–116.

[115] T.A. Vu, G.H. Le, C.D. Dao, L.Q. Dang, K.T. Nguyen, P.T. Dang, H.T.K. Tran, Q.T. Duong, T.V. Nguyen, G.D. Lee, RSC Adv. 4 (2014) 41185–41194.

[116] H. Yang, X.-W. He, F. Wang, Y. Kang, J. Zhang, J. Mater. Chem. 22 (2012) 21849.

[117] C. Jiao, M. Li, R. Ma, C. Wang, Q. Wu, W. Zhi, Talanta 152 (2016) 321–328.

[118] P.Á. Szilágyi, P. Serra-Crespo, I. Dugulan, J. Gascon, H. Geerlings, B. Dam, CrystEngComm 15 (2013) 10175.

[119] L. Shi, L. Yang, H. Zhang, K. Chang, G. Zhao, T. Kako, J. Ye, Appl. Catal. B 224 (2017).

[120] J. Tu, X. Zeng, F. Xu, X. Wu, Y. Tian, X. Hou, Z. Long, Chem. Commun. 53 (2017) 3361–3364.

[121] N.A. Surib, L.C. Sim, K.H. Leong, A. Kuila, P. Saravanan, K.M. Lo, S. Ibrahim, D. Bahnemann, M. Jang, RSC Adv. 7 (2017) 51272–51280.

[122] H. Ramezanalizadeh, F. Manteghi, J. Photochem. Photobiol., A 346 (2017) 89–104.

[123] Q. Yang, Q. Zhao, S. Ren, C. Guo, X.M. Guo, Z. Chen, Polyhedron 122 (2017) 131–136.

[124] T.D. Bennett, A.K. Cheetham, A.H. Fuchs, F.X. Coudert, Nat. Chem. 9 (2016) 11–16.